Department of Hydrology

The Albert-Ludwigs-University Of Freiburg i. Brsg.

By

IMMANUEL FRENZEL

Development of a Snow Module for RoGeR utilizing Clustered Snow Data

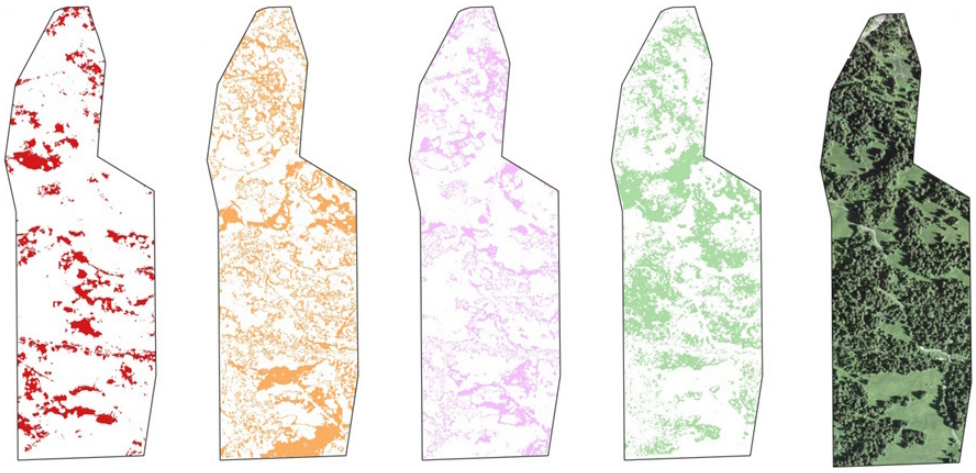

Under the direction of Dr. Prof. Markus Weiler

Supervised by Joschka Geissler

Freiburg i. Brsg., September 2023

Acknowledgements

I would like to express my gratitude to the following individuals for contributing to the completion of my master's thesis:

Giulia Mazzotti, for generously providing the meteorological data that were tested and analysed in this study.

Hannes Leistert, for his diligent efforts in assembling a functional version of RoGeR that was integral in understanding its key functionalities.

Robin Schwemmle, for his dedicated work in constructing a modular RoGeR framework, which will serve for later integration of this works project.

Joschka Geissler, for providing the foundational clustering data upon which this entire work is built. His insightful consultations and inputs greatly enriched the quality of this research.

Markus Weiler, for his expert supervision, guidance, and unwavering support throughout the entire developmental process of this thesis. His expertise played a vital role in shaping the outcome of this work.

Each of these individuals has played their role in the successful completion of this thesis. I deeply appreciate their contributions.

Contents

List of Figures ii

List of Tables ii

Abstract iii

Zusammenfassung iv

1 Introduction 1

1.1 Relevance of Snow Modelling on Different Scales 1

1.2 Modelling Snow Processes 1

1.3 Comparison of Snow Models with Different Complexities 4

1.4 A Way to Reduce Model Complexity - Clustering in Snow Modelling 6

1.5 The RoGeR Model - A short Introduction 7

1.6 Development-Process: A new Snow Model for RoGeR 9

1.7 Research Question 10

2 Methods 11

2.1 The Alptal Test Site 11

2.2 Spatial Cluster Data 11

2.3 Climate Data 12

2.4 Potential Evapotranspiration 13

2.5 Model Development 13

2.6 Goodness of Fit Measures 32

2.7 Parameter Configuration and Model Comparison 33

2.8 Model Output Post-Processing 34

2.9 Creating Accumulation and Ablation Curves 34

2.10 Canopy Layer Evaluation 34

3 Results 36

3.1 Model Parameters, Resolution and Performance 36

3.2 Quantitative Model Evaluation 41

3.3 Accumulation 42

3.4 Ablation 44

3.5 Sublimation 46

3.6 Refreezing 46

3.7 Internal Model Error . . . 46
3.8 Canopy Snow Layer Evaluation . . . 47
3.9 Rain on Snow . . . 48

4 Discussion **51**
4.1 Model Structure . . . 51
4.2 Internal Model Error . . . 51
4.3 Model Parameters . . . 52
4.4 Comparison of Annual Sublimation Values . . . 56
4.5 Hourly and Daily Temperature Input Modelling . . . 57
4.6 Challenges in Rain on Snow Simulation . . . 58
4.7 Evaluation of the Cluster Modelling Approach . . . 59
4.8 Future Research: Enhancing Snow Model Performance . . . 61

5 Conclusion **62**

6 References **64**

7 Appendix **70**
7.1 Climate Graphs . . . 70
7.2 Increase in Precipitation through Richter Correction . . . 71
7.3 Development of the DDF . . . 72
7.4 Sensitivity Analysis . . . 73
7.5 List of supplied Data and Scripts . . . 75
7.6 Abbreviations . . . 76

8 Statutory Declaration **77**

List of Figures

1 Testsite Satellite Image and Clustering Information 12
2 Canopy Liquid Water Routine 27
3 Ground Layer Liquid Water Routine 30
4 Position of SnoMoS 35
5 Model Runs Winter Season 2021/22 38
6 Model Runs Winter Season 2020/21 40
7 Accumlation Processes 43
8 Ablation Processes 45
9 Snow Hours in Canopy 48
10 Model Data for ROS Event 50
11 Appendix: Climate graphs 70
12 Appendix: Variability of the DDF 72
13 Appendix: Dotty Plots 74

List of Tables

1 Input Parameters 15
2 Model Output Variables 16
3 wind speeds for Richter Correction 17
4 Parameters for Richter Precepitation Correction 17
5 Calibration Results 36
6 Goodness of Fit 41
7 Annual Sublimation 46
8 Annual Refreezing 47
9 Internal Model Error 47
10 Validation of Canopy Snow Hours 48
11 Evaluation of a ROS-event 51
12 Appendix: Richter Correction Precepitation Increase 71
13 Appendix: Sensitivity Analysis Parameter Intervals 73

Abstract

Up-scaling snow models has proven to be challenging. A new way of scaling snow simulations could lie in the use of cluster information on snow dynamics. A model calibrated on a small scale could later be up-scaled to wider areas exhibiting the same patterns in snow distribution. Coupled with soil routines this approach could lead to more precise runoff predictions and thereby improve spring-floods and droughts forecasts. For first tests on clustered snow data a snow module is developed for subsequent integration into the Run off Generation Research (RoGeR) program. Model testing is performed with spatially clustered Snow Water Equivalent (SWE) data aiming to reduce model complexity and input parameter count, as well as boosting simulation efficiency. The model's input requirements were streamlined to the most essential components. A straightforward model structure was formulated, employing a dual degree-day-factor (DDF) approach alongside a threshold-based separation for temperature and precipitation. One layer of canopy is simulated. Furthermore, the model incorporates routines for liquid water, refreezing processes, sublimation and Rain on Snow (ROS)-events. The input parameters were set in reasonable boundaries, accurately representing the underlying physical processes. Overall, the model has exhibited commendable performance with only short periods of calibration data. The quality of the outputs is dependent on the resolution of input temperature data. Accumulation and melt rates match the observed SWE when the lack of sublimation in the reference data is accounted for. Annual sublimation and refreezing values match those in literature. The canopy-layer algorithm performs well predicting 95% of the snow hours in south facing canopy correctly. Challenges are faced when simulating ROS-events in forested and open exposed clusters. Future work should include testing with new seasons of input data for the modelled clusters and other clusters in more advanced stages. Later, the model has to prove its structural efficiency while integrating into RoGeR.

Key words: Snow, SWE, RoGeR, Cluster, Model

Zusammenfassung

Die Probleme in der Anwendung von Schneemodellen auf große Flächen sind momentaner Gegenstand der Forschung. Eine neue Möglichkeit zur Skalierung von Schneemodellen könnte in der Verwendung von Cluster-Informationen liegen. Ein auf kleinem Maßstab kalibriertes Modell könnte später auf größere Gebiete mit ähnlichen Schneeverteilungsmustern hochskaliert werden. In Kombination mit Bodenwassermodellen könnte dieser Ansatz zu präziseren Vorhersagen von Abflüssen führen und somit die Vorhersagen für Hochwasser und Dürre verbessern. Ein Schneemodul zur späteren Integration in RoGeR wurde entwickelt. Kalibrierung und Validierung erfolgte anhand von räumlich gruppierten Daten zur Schnee-Wassermenge (SWE), um die Modellkomplexität und die Anzahl der Eingangsparameter zu reduzieren und die Simulationseffizienz zu steigern. Die Eingangsanforderungen des Modells wurden auf die wesentlichen Komponenten beschränkt. Es wird eine einfache Modellstruktur formuliert, die einen dualen Grad-Tag-Faktor(DDF)-Ansatz neben einer schwellenbasierten Trennung für Niederschlag verwendet. Zusätzlich zur Bodenschneedecke wird die Schneemenge im Blätterdach simuliert. Darüber hinaus enthält das Modell Routinen für flüssiges Wasser, Wiedergefrierungsprozesse, Sublimation und Regen auf Schnee (ROS)-Ereignisse. Die Eingangsparameter wurden in Grenzen festgelegt, die die zugrunde liegenden physikalischen Prozesse abbilden. Insgesamt zeigt das Modell gute Leistung mit nur kurzen Kalibrierungszeitreihen. Die Qualität der Ergebnisse hängt von der Auflösung der Eingangstemperaturdaten ab. Die Akkumulations- und Schmelzraten stimmen mit der beobachteten SWE überein, wenn der Mangel an Sublimation in den Referenzdaten berücksichtigt wird. Die jährlichen Sublimations- und Wiedergefrierungswerte entsprechen denen in der Literatur. Der Algorithmus für die Schneeschicht in Bäumen liefert gute Ergebnisse und kann 95 % der Schnee-Stunden in südlich ausgerichteten Baumbeständen korrekt vorhersagen. Herausforderungen ergeben sich bei der Simulation von ROS-Ereignissen in bewaldeten und exponierten Clustern. Zukünftige Arbeiten sollten Tests mit neuen Wintern für die modellierten Cluster und anderen Clustern in fortgeschritteneren Stadien einschließen. Später soll das Modell auf seine strukturelle Kompatibilität bei der Integration in RoGeR getestet werden.

Schlüsselwörter: Schnee, SWE, RoGeR, Cluster, Modell

1 Introduction

1.1 Relevance of Snow Modelling on Different Scales

Snow processes play a crucial role in the hydrological cycle, impacting various aspects of the environment. Snow models have been developed to quantify and predict these processes. This is essential for understanding and adapting to the changing climate on various spatial scales.

On a scale of small to medium sized catchments, sudden snow melts induced by rain are a major cause of spring floods. The frequency of flood events caused by rain on snow in the European Alps has been increasing over the last decades. Accurate prediction of rain on snow events is vital for effective flood management and mitigation of the emerging risks (Garvelmann 2014; Beniston and Stoffel 2016).

In large catchments insufficient snowfall and premature snow melt have led to severe summer droughts in Europe. This is exemplified by the 2022 drought across the Po river basin in northern Italy. Such events are becoming more common, emphasizing the need to quantify water deficits, and implementing effective countermeasures (Iglesias, Assimacopoulos, and Van Lanen 2018) (Toreti et al. 2022).

Those phenomena are linked to a changing climate. Globally the duration of snow cover influences the Earth's albedo, providing a direct counterbalance to global warming. Other climate tipping points are related to snow dynamics. This is exemplified by the snow coverage's influence on the CO_2 emissions of vast areas of permafrost soils, indirectly reducing the greenhouse effect (Jorgenson et al. 2010) (Natali et al. 2019).

1.2 Modelling Snow Processes

Various processes are included in state-of-the-art physically-based snow modules to match reality as close as possible:

Distinction between liquid and solid precepitation can be made by using a threshold temperature. A meta-analysis of a comprehensive 29-year observational dataset reveals substantial variations in the air temperature at which rain and snow occur with equal frequency across the Northern Hemisphere. On average, this temperature stands at 1.0°C, but it exhibits a considerable range

from -0.4°C to 2.4°C for 95% of the monitoring stations (Jennings et al. 2018).
A more advanced way of identifying snowfall is a Wet-Bulb-Temperature approach. In addition to temperature and precipitation, relative humidity is needed for this calculation. This method of solid-liquid precipitation separation performs superior to the threshold temperature approach overall (Behrangi et al. 2018).

Fresh fallen snow differs in its physical properties. For the estimation of fresh snow density various methods exist, using air-temperature and wind speed as input data (Hedstrom and Pomeroy 1998) (Jordan, Andreas, and Makshtas 1999) (Davidov et al. 2004). The empirically-based approach after Hedstrom using only air temperature for fresh snow density calculation has been shown to perform well under various conditions (Zhibang and Pomeroy 2020).

Fresh snow is intercepted in canopy when present. The amount of interception during a snow event is dependent on the fresh snow density, the maximal amount of intercepted snow, the initial amount of intercepted snow, the Leaf Area Index (LAI), the canopy-coverage, the canopy-height and lastly wind-speed and wind-direction. A widely used approach for modelling interception for boreal forests, using most of the named influencing factors as input parameters is available (Hedstrom and Pomeroy 1998). A more simplistic way of calculating interception was used in the ITree-Hydro model (Yang, Endreny, and Nowak 2011): The percentage of snow which is intercepted by the canopy is calculated by an exponential term including the LAI and an extinction coefficient in the exponent. This calculation was transferred from liquid precipitation interception modelling.

Intercepted snow is unloaded from canopy due to wind and changes in the structure of the intercepted snow, dependent on temperature and radiation. This process is often modelled using an exponential decay of the interception snow storage, determined by an unloading coefficient (Hedstrom and Pomeroy 1998). Approaches including temperature or radiation-balance components are present in the literature (Mahat and Tarboton 2014) (Förster et al. 2018) as well.

Besides unloading, snow is also removed from canopy by sublimation. Up to 30% of fallen SWE was reported to be returned to the atmosphere by sublimation in boreal forest (J. W. Pomeroy and Schmidt 1993). Other sources report values from 36.4% to 80.7% for more arid climates (Voordendag et al. 2021). This process is dependent on windspeed, relative humidity, radiation, temperature, air pressure, physical parameters of the canopy snow layer and structural canopy parameters such as height, LAI and canopy coverage. For calculation an energy balance of the canopy snow layer is set up in order to determine the amount of energy available for sublimation

(J. Pomeroy et al. 1998) (Mahat and Tarboton 2014). For calculating the amount of incoming short-wave radiation absorbed by the snow layer, an algorithm for albedo calculation is required.

The formation of rime ice is a canopy process that was only recently described for the first time (Lumbrazo et al. 2022). Rime ice is created when powerful winds transport supercooled water droplets from clouds causing them to accumulate on surfaces. Typically, rime formation takes place under specific conditions, including high wind speeds, elevated humidity levels, and air temperatures ranging between -2°C and -8°C (Whiteman and Garibotti 2013). The magnitude of the impact on intercepted snow is still to be evaluated. Furthermore the canopy modifies various parameters important for snow modelling. Windspeed in the canopy is reduced. Shading effects modify radiation heterogeneously. Snow is distributed unevenly due to spatial patterns in the canopy layer (Zheng et al. 2018).

Modelling of melt for the canopy and ground snow cover follows the same principles for canopy and ground, with modifications as described when canopy is present. Two basic approaches can be distinguished: A DDF-method and an energy balance calculation. The degree-day method calculates melt based on a factor determining how much snow is melted dependent on temperature above zero degrees Celsius per day. This calculation is used in many models due to its simplicity. One of the most prominent members of this group is the NORDIC HBV model (Saelthun 1996). Energy balance models calculate the energy fluxes within the snow layer and on its surface. The first part of the energy balance is radiation. Therefore, data for incoming shortwave radiation is needed. Reflected shortwave radiation is calculated based on a modelled albedo for the snow surface. Longwave radiation can be determined by atmospheric and snow temperature. The second part is heat fluxes on the surface of the snow layer. Heat is conducted from or to the soil. For modelling, soil temperature and a heat conductivity calculation within the soil (dependent on water content and density) are needed. On the upper surface heat is exchanged with the atmosphere. Turbulent heat exchange prediction additionally needs windspeed, air pressure and relative humidity. Latent heat is transported due to sublimation and freezing processes on the surface of the snow layer. Finally falling rain adds energy to the snow cover depending on its temperature. An algorithm able to perform all these calculations is the FSM model (Essery 2015). The Snow Model Intercomparison (SNOW-MIP) meta study evaluated the degree-day method as well as the energy balance method (Krinner et al. 2018; Essery et al. 2009; Etchevers et al. 2004). Model performance was not dependent on the chosen melt-modelling approach.

Melting water and rainwater are stored in the snow cover to a certain extent. Values for the maximum liquid water storage found in literature reach from 4 % (Koch et al. 2014) to over 6% (Mitterer et al. 2011) (of SWE). The holding capacity depends on the physical properties of the snow layer. Simpler modelling approaches fix the maximum liquid storage to a certain fraction of the SWE. For example, the Nordic HBV model uses a value of 8% (Saelthun 1996). The stored liquid water is refrozen when temperatures drop below freezing. This can be estimated using a method like the DDF called refreezing efficiency. A fraction of liquid water refreezes. The amount is depending on the refreezing efficiency multiplied with the DDF and the value of temperature below zero. For precise modelling a temperature calculation for the snow cover is necessary. This is already present within most energy-based models. Field studies for quantifying refreezing were mostly conducted on glaciers and in arctic regions. On the Greenlandic ice shield, more than 50% (Cox, Humphrey, and Harper 2015) of melt water is retained and refrozen in the firn layer. For moderate climates no estimates for refreezing could be retrieved. Overall water content is of great importance when forecasting flash floods caused by rain on snow events (Li et al. 2019) and in avalanche forecasting. For avalanche risk evaluation, complex 3D models with multiple snow layers have been developed. An example is the Alpine 3D model, developed by the Swiss WSL-Institute for Snow and Avalanche Research SLF (Lehning et al. 1999).

This model is also able to handle snow drift calculations. Therefore, a high resolution digital-elevation-model in combination with an algorithm for small scale modelling of windspeeds is needed.

Overall, many snow processes can be modelled with a pool of input parameters to choose from. Model complexity depends on the parameters chosen and on the selection of processes modelled. Both decisions are depending on the desired model application. The availability of input data determines the amount of the processes the model is able to simulate.

1.3 Comparison of Snow Models with Different Complexities

The issue at hand is: What level of complexity is necessary to accurately describe the relevant snow processes? Some models adopt simpler approaches that do not explicitly consider vegetation processes. As part of the Project for the Inter-comparison of Land Surface Parametrization Schemes (PILPS) (A. Henderson-Sellers et al. 1995), an initial examination of various snow models was conducted. The PILPS 2(d) Project evaluated 21 snow models using an 18-year dataset from

a grassland catchment in Russia. The results revealed significant variation among the models, particularly during the early snow season and ablation events. This discrepancy was attributed to the diverse energy distribution among the snow-covered grid cells under low-SWE conditions. Biases established early in the snow season persisted due to internal feedback processes or independent snowfall events (Slater et al. 2001). At that time, including vegetation influences was still deemed necessary.

Two years later, the SnowMIP project was initiated (Etchevers et al. 2004) with the goal of developing a methodology for comparing different snow models. The project focused on mountainous catchments in the Alps but did not consider vegetation patterns. The project emphasized the importance of accurately calculating albedo, as it significantly affects radiation balance. Many of the 23 surveyed models encountered challenges in precisely determining the available energy in the snow cover due to the albedo calculation.

Six years later, the project was repeated to evaluate model performances in forested catchments (Essery et al. 2009). A wide range of snow models was tested across three forested catchments at altitudes ranging from 579 to 2820 meters. The complexity of the models varied, from simply reducing snowfall due to vegetation to a 10-layer interception snow model. All 33 models performed well in predicting the duration of snow cover but struggled to accurately model maximum snow accumulation. Specifically, they underestimated the differences between forested and non-forested sites, particularly in warmer winters. However, improvements were noted in albedo calculations. Overall, the study concluded that uncertainties in parameter selection are more important than deficiencies in model structure in the absence of calibration data (Essery et al. 2009). It was suggested that snow models should be tested on a larger scale.

The most recent assessment of snow models, ESM-SnowMIP (Krinner et al. 2018), addressed the need to bridge the gap between research groups, focused on small-scale snow modelling, and researchers in earth system modelling. The study aimed to establish standardized experiments for comparing snow models.

The study concluded: there are problems due to error accumulation in snow modules. This is especially true for warmer winters. Canopy modelling is still challenging, and uncalibrated models still do not perform well. The model quality hugely depends on the selection of input parameters.

1.4 A Way to Reduce Model Complexity - Clustering in Snow Modelling

Currently, research is conducted in up-scaling hyper-scale models to improve snow modelling efficiency. That involves the utilization of intricate energy balance models. Good results have been achieved using the FSM (Mazzotti, Essery, Webster, et al. 2020; Mazzotti, Essery, Moeser, et al. 2020). The process of up-scaling these models has proven to be quite challenging (Mazzotti et al. 2021). Aiming to solve these problems in snow modelling, a new way of snow depth calculation in clusters was proposed by Geissler, Rathmann, and Weiler (2023). This work is mainly based on the data generated in that study. High resolution LiDAR snow depth maps (HS-maps) and a network of Snow Monitoring Stations (SnoMoS) (Garvelmann 2014) at a sub-alpine test site in Switzerland were evaluated. Four clusters of snow depth could be identified: Open shaded, open exposed, open intermediate and forested. Eventually those clusters could be derived from satellite data. If modelling those clusters is more efficient than modelling whole country sights a huge step in snow modelling can be made. Modelling clusters instead of grid cells reduces the model-runtime significantly. Furthermore, relevant processes could be chosen individually for each cluster. Therefore, model complexity could be reduced to the amount necessary for each cluster. Potentially this leads to fewer input parameters. Parameters for vegetation and topography are available on small experimental sites. The same is true for high-resolution climate data. The lack of such data on a global scale poses a significant challenge when integrating snow models into Earth System Models (ESM). This integration is crucial for generating accurate snow cover predictions and assessing the impact of climate change on melting ice sheets, glaciers, and snowfall (Krinner et al. 2018). Together these achievements (fewer input data, simpler parametrisation, lower computation times due to simpler model designs) could help with up scaling the model to wider areas and improving model results of snow models.

1.5 The RoGeR Model - A short Introduction

To address the introductory application areas of snow modelling, snow modules are often coupled with runoff-generation modules. Available for this work is the RoGeR model. Input parameters are time series for precipitation temperature, potential evapotranspiration and incoming short wave radiation in some variants.

To estimate flood and drought events, runoff generation modelling is necessary. RoGeR simulates runoff formation with high temporal resolution based on physical principles. The drainage components considered include Hortonian surface runoff, rapid interflow through preferential flow paths, slow interflow through the soil matrix, surface runoff on saturated areas, and deep percolation into groundwater. The model captures the infiltration process through the soil and accounts for infiltration through macropores and dry cracks. The event-based runoff generation models of RoGeR can be applied at any time step. The water balance models adjust the time step between ten minutes, one hour, and one day during the model run, depending on the rainfall intensity. This ensures that the effects of short-term high intensities are considered even for model runs spanning several years. For low intensities, an hourly time step is sufficient, and if there is no rainfall, calculations are performed daily (Steinbrich, Weiler, and Leistert 2021).

For drainage concentration modelling, two alternative methods are available. The first is a geomorphological unit hydrograph approach. This involves deriving a unit hydrograph for each of the three components: surface runoff, interflow, and deep percolation (groundwater runoff). This allows for the derivation of a hydrograph for each component at any point in the catchment. The second approach is modelling the concentration of surface runoff and interflow dynamically. This considers both the falling rainfall and the laterally inflowing water at each time step in the infiltration modelling. For surface runoff, a 2-D explicit method is used to solve the diffusive wave equation in combination with the Manning-Strickler equation. A similar approach is applied to interflow, but in combination with Darcy flow and preferential lateral interflow. For each cell, the water available locally for interflow formation from the soil and the laterally inflowing water are considered. In dynamic modelling, it is no longer possible to differentiate between the various drainage components at the gauge. Especially during short intense rainfall events, the infiltration of surface runoff along the flow path has a significant impact compared to the unit hydrograph approach. Since more water infiltrates overall, the resulting drainage response at the gauge is weaker. In recent tests,

the dynamic modelling showed a reduction in drainage compared to the unit hydrograph approach ranging from 15 to 75% at the gauge (Steinbrich, Weiler, and Leistert 2021).

RoGeR is able to consider the evaporation from water surfaces, interception storage in the tree canopy as well as separately from the shrub and grass layers (including areas under canopy) and from the soil itself. The potential evaporation, defined as a daily input, is reduced based on water availability and shortwave radiation. The potential evaporation is available in two layers in the model: at the ground- and in the grass- and shrub- layers as well as in the tree layer. This allows for the possibility of actual evaporation being higher than the potential evaporation. The radiation input can be reduced due to shading, which can be considered in the raster-based model versions using shading grids that vary with the seasons (Steinbrich, Weiler, and Leistert 2021).

Soil water storage is defined by the parameters field capacity, air capacity, drainable porosity, and permanent wilting point. The soil is divided into the root zone and the soil below the root zone. Evaporation from the soil only occurs from the root zone. There is an exchange of water between the two soil zones based on the matrix potential. Water can be released from the subsoil to the underlying geological layer (deep percolation) depending on the water content. This water corresponds to groundwater recharge. Capillary rise is also possible at high groundwater levels. If the field capacity is exceeded, a saturated zone can develop above it, depending on the permeability of the geological substrate. Interflow occurs in this zone. The amount of interflow depends on the lateral permeability of the soil at the base, the depth of the soil, and the slope. Preferential lateral flow paths in this zone are parameterized in RoGeR based on land use and soil skeleton content (Steinbrich, Weiler, and Leistert 2021).

1.6 Development-Process: A new Snow Model for RoGeR

In the pursuit of developing a snow module that seamlessly integrates into the RoGeR program, several significant factors become prominent. This study aims to clarify the essential elements required for constructing an effective snow module for RoGeR, emphasizing efficiency and practical usefulness. At the core of this research lies the vital role of thorough documentation, which not only aids in current understanding but also establishes the foundation for future collaboration and integration.

An important aspect of concern involves managing external dependencies. This calls for a selective integration of external tools to ensure alignment with RoGeR's overarching framework. Moreover, leveraging RoGeR's existing input data – including temperature, precipitation, and evapotranspiration – forms a foundational element in this endeavour. The goal is to harmoniously incorporate this data into the snow module, creating a coherent relationship with RoGeR's inherent operational structures.

Most importantly RoGeR uses variable time stepping. Therefore the model has to incorporate this feature in order to run alongside RoGeR. This adaptable temporal resolution not only enhances the module's flexibility, but also broadens its applicability across diverse environmental scenarios. Testing the model with different temporal resolutions will help with the fine tuning of RoGeR's time-stepping routine later on.

Furthermore, the meticulous creation and provision of comprehensive model output data hold significant importance, guaranteeing the availability of an extensive dataset for subsequent analytical insights.

A central focus of this research pertains to the systematic establishment and documentation of an interface facilitating seamless data exchange between the snow module and RoGeR. In principle the snow module should be operable with other runoff-generation models trough the interface.

The last aspect revolves around aligning the structural design of the snow module with RoGeR's fundamental computational paradigm, characterized by its iterative 'for-loop' architecture. This alignment streamlines the incorporation of the snow module's functionalities within RoGeR's iterative framework, resulting in a cohesive and synergistic simulation framework.

In summary, this study aims to break down the complex landscape underpinning the development of a snow module for RoGeR, with a strong focus on detailed documentation, prudent selection of tools, seamless data integration, adaptive time resolution, comprehensive output provision, interface management, and structural alignment.

1.7 Research Question

The objectives of this master's thesis are twofold: firstly, to undertake the development of an efficient snow module for the RoGeR program. This entails a comprehensive consideration of key factors, including modular integration, minimal external dependencies, effective utilization of available RoGeR input data (temperature, precipitation, evapotranspiration), dynamic temporal resolution, and robust data output provisions.

Secondly, this research seeks to evaluate the newly developed snow module using clustered sample data derived from the two year Geissler, Rathmann, and Weiler (2023) dataset. This research should focus on the differences in snow processes in between the clusters. Furthermore, an assessment of the potential disadvantages of modelling with daily temperature inputs should be conducted.

By achieving these two goals, this work aims to make contributions towards an advancement of both the RoGeR program and the broader field of snow modelling.

2 Methods

2.1 The Alptal Test Site

The test site is located on a hillside of the Alptal valley in Switzerland. Situated at geographical coordinates 47.044380, 8.712755 (EPSG:3857), the test site is forested by a mixed composition of spruce and fir trees. Exhibiting an LAI ranging from 4 to 5 m^2/m^2 the test site canopy reaches heights of up to 35 m with a mean canopy coverage of 35%. The test side is orientated no-break space, encompassing an azimuthal range from 211° to 296°. Topographically, the undulating terrain showcases slopes ranging from 11° to 25°. The elevation of the test site spans from 1160 meters to 1240 meters above mean sea level (m.a.s.l.). The whole test site covers an area of approximately 0.23 km^2 (Geissler, Rathmann, and Weiler 2023).

2.2 Spatial Cluster Data

Daily SWE raster stack data were obtained from the FreiDok Repository (https://doi.org/10.6094/UNIFR/232647). For creating the data set an unmanned aerial vehicle (UAV) equipped with a VLP16 Puck Lite multi-beam LiDAR sensor and an inertial navigation system was used to carry out aerial surveys to collect data on snow depth and SWE in the study area. The UAV surveys were carried out throughout the seasons, allowing for the measurement of snow depth during different stages of the snowpack. The collected LiDAR data was processed to generate high-resolution snow-depth maps (HS-maps) of the snow-covered area . To fill the data gaps in the LiDAR surveys, data imputation was used. The UAV surveys were complemented by manual snow surveys, where snow depth and SWE measurements were taken along transects within the study area. Additionally, the LiDAR data were supplemented with data of a dense sensor network of automatic Snow Measuring Stations (SnoMoS). The k-means clustering algorithm was used to detect clusters in a randomly chosen subset of the HS-maps data, which were then used as target variables in a random forest classification. Therefore the HS-maps were split in four maps each for model training and calibration. The model results are later validated with the remaining two maps. The resulting maps provided allocation probabilities for each cell to the respective cluster. Those were combined with the temporal information from the snow surveys to estimate daily snow depth for each cell (daily HS-maps). This was done using the normalized probabilities of all SnoMoS

belonging to a cluster. Multiplying the probability to the SnoMoS time series results in HS-time series for each cluster. Daily HS-maps are created by the summed product of probability and the corresponding cluster HS-time series for each cell. The clusters found are visualized in Figure 1. For deriving daily SWE-maps from the daily HS-maps the semi-empiric ΔSnow Model was used (Winkler, Schellander, and Gruber 2021). The model is able to derive the SWE only relying on a HS time series. Mean associated errors show high correlations when compared to the manually taken snow data for HS-maps (R = 0.95) and for SWE-maps (R = 0.89) (Geissler, Rathmann, and Weiler 2023).

For this work the modelled SWE-maps are used together with the clustering information. Therefore, daily SWE-maps are cropped to each cluster and mean daily values are taken. Cropping and summarising is done using the raster-package (R 4.2.0, Hijmans (2023)). The code is provided in the digital appendix of this thesis.

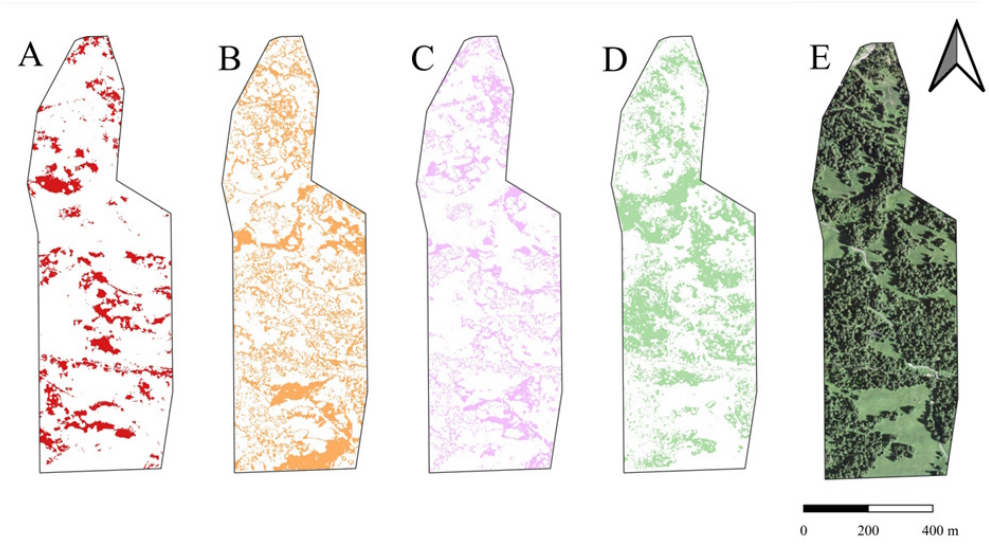

Figure 1: Clustering information for the clusters open exposed (A), open shaded (B), open intermediate (C) and forested (D) by Geissler, Rathman, and Weiler 2023. (E) shows a satellite image of the testsite

2.3 Climate Data

Hourly climate data from the test site's meteorological station Erlenhoehe are available as well as measurements for temperature, precipitation, relative humidity, incoming shortwave radiation and wind speed. The climate input is attached to this document. The data is manually corrected by Weiler (2023). From the two precepitation time series available, the "NS" time-series was selected. The dataset was screened for duplicated entries, zero were found. Negative values for shortwave

radiation (48%) were set to zero. Missing values for temperature (0.09%), shortwave radiation (17.03%) and relative humidity (0.08%) were filled with monthly means. Datetime (year, month, day and hour), temperature, precipitation and evapotranspiration are selected as model input. The raw and cleaned data is attached to this thesis. Climate data wrangling was performed using the tidyverse-package (R 4.2.0, raster-package Wickham et al. (2019)). The lubridate package (R 4.2.0, Grolemund and Wickham (2011)) is used for datetime calculations. A climate graph for the whole winter seasons 2020/21 and 2021/22 can be found in Figure 11 (Appendix).

2.4 Potential Evapotranspiration

Data were aggregated to daily values (R 4.2.0, tidyverse-package) to calculate daily evapotranspiration (R 4.2.0, evapotranspiration-package (Guo, Westra, and Maier 2016)). The provided ET.Penman-method was used with the following set of parameters:

- solar="data"
- wind="yes"
- windfunction_ver=1948
- alpha=0.08
- z0=0.001

The calculation is based on the original Penman equation (Penman and Keen 1948). Code to produce the climate-input data can be found in the supplementary data of this work.

2.5 Model Development

2.5.1 Overall Structure

The module is designed as a callable function. Input and configuration parameters must be provided by RoGeR. This includes the initial SWE before each time step, temperature, evapotranspiration, precipitation and the model configuration. A list of all inputs can be found in the chapter Input Data. Model output must be stored in RoGeR or is lost otherwise.

2.5.2 Python Environment

Programming was done in a python environment (Python 3.11). The code is edited with PyCharm community edition Version 2023.1. Packages loaded are:

- numpy for efficient calculations in the numpy array data structure (Harris et al. 2020)
- pandas for input and output data wrangling in dataframes (McKinney and Others 2010)
- datetime for date and time formatting inside the module (Python Software Foundation 2021)
- solarpy for complex radiation input calculations (AeroPythonTeam 2019)

2.5.3 Input Data

Input data for the snow module function are month, day, hour, minute and second to calculate a seasonal dependent radiation influence on the DDF. Only year, month and day are mandatory. Temperature, snowfall temperature, a base DDF and precipitation are necessary to determine various accumulation and melt processes. The potential evapotranspiration is needed for an adjusted sublimation calculation. A time step input allows variable time-stepping. Initial values for SWE and liquid content (canopy- and ground-layer) before the next model time step should be provided. A storage coefficient gives a fraction of liquid water which can be stored in the snow-layer. An unloading factor determines the fraction of snow unloaded per day. Canopy coverage and a leaf area index adjust the behaviour of ground and canopy layer. A shade value influences the extent of the radiation impact on the DFF. This should be used to quantify shading through mountains or nearby canopy. The refreezing rate determines the amount of refreezing dependent on the DDF. Elevation, latitude, slope and aspect are necessary for incoming solar radiation calculations. The station exposure variable is needed for precipitation correction. All input values are listed in Table 1.

2.5.4 Output Format

The model output is a named numpy array containing the values shown in Table 2. Primarily relevant for RoGeR are the ground layer outflow and model state variable. They determine if RoGeR evaporation calculations should be turned on or off. When off, the evaporation calculations

Table 1: Overview of all input parameters of the snow module

Model Variable	Description	Default	Unit
year	Year (YYYY)	-	-
month	Month (1-12)	-	-
day	Day (1-31)	-	-
hour	Hour (00 - 23)	0	-
minute	Minute (00 - 59)	0	-
t	Temperature	-	-
precip	Precipitation for the time step	-	-
et	Potential daily Evapotranspiration	-	-
timestep	Time step	60	min
swe_canopy_0	Initial snow cover in the canopy as SWE	0	mm
swe_ground_0	Initial snow cover on the ground as SWE	0	mm
liquid_content_canopy_0	Initial liquid content in the canopy	0	mm
liquid_content_ground_0	Initial liquid content on the ground	0	mm
storage_coef	Faction of the snowcover of maximum liquid storage (0-1)	0.08	-
unloading_factor	Unloading per day as a fraction of initial load (0-1)	0.1	-
canopy_coverage	Coverage of the canopy as fraction (0-1)	0	-
ddf	Base-DDF	1.5	mm/C/day
t_snowfall	Temperature dividing between snow and rain	0.5	C
shade	Factor regulating the radiation effect on the DDF (1: No radiation, 0: Full radiation)	0.5	-
lai	Leaf area index for canopy, zero if no canopy present	4	-
refreezing_rate	Refreezing efficiency (dependent on DDF)	1	-
elev	Elevation	500	MSL
lat	Latitude	45	degree
slope	Mean Slope of the ground surface	0	degree
aspect	Mean Aspect of the ground sourface	180	degree
station_exposure	Station exposure derived from mean windspeed	0	-

should be left to the sublimation routine of the model. Additional variables are supplied in the output for later analysis.

2.5.5 Model State

The model state determines if the model is turned on or off. If the initial SWE for ground and canopy layer are zero and the temperature is above snowfall threshold the snow module is turned off. For the sake of a faster runtime no calculations are made in this case. Otherwise, the model state is in "on" position. This is important for communication with RoGeR. For a model state "on", RoGeR should turn off evaporation and interception calculations. Additionally precipitation

Table 2: Output data format of the snow module

Variable	Datatype	Description	Unit
interception_storage	float	Storage available for intercepting snow	mm
ddf_canopy	float	DDF for canopy melting	mm/d/°C
ddf_ground	float	DDF for ground melting	mm/d/°C
interception	float	The actual amount of interception	mm
accumulation_canopy	float	Accumulating snow in canopy	mm
rain_canopy	float	Precipitation reaching the canopy snow layer	mm
accumulation_ground	float	Accumulating snow on ground	mm
rain_ground	float	Precipitation reaching the ground snow layer	mm
melt_pot_canopy	float	Potential melt in canopy layer	mm
melt_pot_ground	float	Potential melt on ground	mm
rain_melt_pot_canopy	float	Potential melt due to rain in canopy	mm
rain_melt_pot_ground	float	Potential melt due to rain on ground	mm
sublimation_pot_canopy	float	Potential sublimation in canopy	mm
sublimation_pot_ground	float	Potential sublimation on ground	mm
swe_canopy	float	Stored snow water equivalent in the canopy	mm
sublimation_canopy	float	Actual sublimation in the canopy	mm
melt_canopy	float	Melting in canopy	mm
rain_melt_canopy	float	Rain melt in canopy	mm
swe_ground	float	Stored snow water equivalent on ground	mm
sublimation_ground	float	Actual sublimation on ground	mm
melt_ground	float	Melting on ground	mm
rain_melt_ground	float	Rain melt on ground	mm
swe_canopy_unloaded	float	Amount of unloaded snow from the canopy	mm
dripping	float	Amount of liquid water emitted by the canopy layer	mm
liquid_content_canopy	float	Amount of liquid water stored in the canopy snow layer	mm
outflow_ground	float	Water reaching the ground surface	mm
liquid_content_ground	float	Amount of liquid water stored in the ground snow layer	mm
refreezing_canopy	float	Amount of water refreezing in canopy	mm
refreezing_ground	float	Amount of water refreezing on the ground	mm
model_state	int	Returning the model state, 1-Model on, 0-Model off	-

input should be directed into the snow module. Outflow from the ground-snow layer serves as input for the RoGeR ground module.

2.5.6 Richter Precipitation Correction

Precipitation is separated in four categories following Richter (1995): liquid summer, liquid winter, mixed and snowfall. Summer and winter precipitation are separated by month, setting May to October as summer months. Mixed precipitation occurs between 0.5 °C ± snowfall temperature. Above this range precipitation is counted as liquid (summer or winter), below as snowfall. A corrected precipitation value is calculated as shown in Formula 2.1. The meteorological station Erlenhöhe is rated as heavily sheltered (Table 4) due to a mean wind speed of 1.24 m s^{-1} for the years 2021 and 2022.

$$P_{corr} = P + b \times P^{\epsilon} \tag{2.1}$$

P_{corr} = Richter corrected precepitation [mm]

P = Measured precipitation [mm]

b = Richter value for station-exposure-type [-]

ϵ = Richter value for precipitaion-type [-]

Table 3: Categorization of meteorological stations by mean wind speed (Richter 1995) and the input code for the model.

Windspeed	Exposure	Input
0-2 m/s	heavily sheltered	4
2-5 m/s	moderately shelterd	3
5-8 m/s	slightly shelterd	2
>8 m/s	exposed	1

Table 4: Parameters ϵ and b for Richter precepitation correction (Richter 1995)

		b			
type	ϵ	exposed	slightly sheltered	moderately sheltered	heavily sheltered
liquid summer	0.38	0.34	0.31	0.28	0.24
liquid winter	0.46	0.34	0.28	0.24	0.19
mixed	0.55	0.54	0.39	0.30	0.18
snow	0.82	0.72	0.51	0.33	0.21

2.5.7 Evaporation Enthalpy

The model is equipped with a routine for estimating the temperature dependent evaporation enthalpy for liquid water after B. Henderson-Sellers (1984) shown in Formula (2.2). By adding a melt enthalpy of 2.26 MJ kg^{-1} a sublimation enthalpy is calculated. The assumption is made that 1 kg of liquid water equals 1 L (or 1 mm water height normalized on 1 m^2).

$$H_{evap}(T) = 1.91846 \times 10^6 \times \left(\frac{T}{T - 33.91}\right)^2 \tag{2.2}$$

H_{evap} = Evaporation Enthalpy [J kg^{-1}]

T = Temperature [K]

2.5.8 Maximum Interception Storage

To consider unloading an interception processes, an interception storage for snow is estimated. Therefore, Formula (2.3), developed from Schmidt and Gluns (1991) and expanded by Hedstrom and Pomeroy (1998) was used. A factor for canopy coverage is added. To compute the snow density of fresh falling snow needed for the calculation, Formula (2.4) was obtained from the US-Army-Corps-of-Engineers (1956).

$$I_s = 6 \times LAI \times cc \times \left(0.27 + \frac{46}{\phi}\right) \tag{2.3}$$

$$\phi = 67.92 + 51.25 \times \exp\left(\frac{T}{2.59}\right) \tag{2.4}$$

I_s = Interception storage [mm]

LAI = Leaf Area Index [-]

cc = Canopy Coverage [-]

ϕ = Density of freshly fallen snow [g cm^{-3}]

T = Temperature [°C]

2.5.9 Degree-Day-Factor

For this model the DDF is split into two components, loosely following the path suggested by Hock (1999). A fixed base value accounting for non-seasonal influences. A variable term accounts for incoming shortwave radiation. This is done using the solarpy package (Python 3.11, AeroPython-Team (2019)) to calculate potantial global radiation. The calculation is based on a solar model from Duffie (1974). Latitude, slope, elevation and aspect are taken into account. This is done for the start and the middle of each time step. Both values are averaged to ensure good representation of the radiation for time steps up to one day. Finally radiation is reduced by a mean transmittance ($T = 0.75$, (Hock 1999)). Then reflection on the snow surface is applied. The albedo for melting snow was estimated to 0.4 according to Conway, Gades, and Raymond (1996) and Becherini et al. (2021). Global radiation values, ranging from zero to 1.2×10^3 Wm^2 are multiplied with a factor of 4×10^{-2} to get a proper representation of a seasonal DDF, as proposed by Hock (1999). The whole equation is shown in Formula (2.5). DDF values are calculated differently for forested and barren landscapes. Even if there is little to no canopy present directly at the site, shading can occur due to nearby canopy. In this case the shading value reduces the radiation part of the ground layer DDF (Formula (2.6)). For forested areas, the DDF below canopy is automatically reduced by shading calculated out of canopy coverage. Canopy DDF is calculated as shown in Formula (2.6).

$$G_{mean} = \frac{G_{start} + G_{middle}}{2} \tag{2.5}$$

$$DDF_{annual} = G \times rrf \times k \times (1 - a)$$

G = Potential global radiation [kW m^{-2}]

DDF_{annual} = Seasonal part of the DDF [mm $^{\circ}\mathrm{C}^{-1}\mathrm{d}^{-1}$]

rrf = Radiation reducing factor set to 0.04 [-]

k = Mean Transmittance estimated to 0.75[-]

a = Albedo of melting snow estimated to 0.4 [-]

$$DDF_{ground} = [DDF_{base} + DDF_{annual} \times (1 - cc) \times (1 - shade)] \times ts \quad (2.6)$$

$$DDF_{canopy} = (DDF_{base} + DDF_{annual}) \times ts \quad (2.7)$$

DDF_{ground} = DDF for groundlayer [mm °C^{-1} d^{-1}]

DDF_{base} = Fixed part of the DDF [mm °C^{-1} d^{-1}]

cc = Canopy Coverage [-]

$shade$ = Shading 0: No shading, 1: Full shading [-]

ts = Time step [d]

DDF_{annual} = Seasonal part of the DDF [mm°C^{-1} d^{-1}]

DDF_{canopy} = DDF forcanopy layer [mm °C^{-1} d^{-1}]

2.5.10 Interception

Interception is estimated based on an algorithm described by Hedstrom and Pomeroy (1998). Intercepted snowfall is calculated as shown in Formula (2.8).

$$I = cc \times p \times \frac{I_s - SWE_{0,c}}{I_s} \quad (2.8)$$

I = Interception [mm]

cc = Canopy Coverage [-]

p = Precepitation [mm]

I_s = Interception storage [mm]

$SWE_{0,c}$ = Initial SWE stored in canopy [mm]

2.5.11 Accumulation

The accumulation routine separates solid and liquid precipitation. Snow and rain (Formula (2.9) and (2.10)) are distributed to ground- and canopy-layer. The amount of intercepted rain in the canopy snow layer is assumed to be equal to the precipitation values multiplied with canopy coverage. The rain part will be used for rain on snow melt calculations later on.

$$acc_{ground} = \begin{cases} p - I & \text{for } T \leq t_{snow} \text{ and } LAI \neq 0 \\ p & \text{for } T \leq t_{snow} \text{ and } LAI = 0 \end{cases} \tag{2.9}$$

$$acc_{canopy} = \begin{cases} I & \text{for } T \leq t_{snow} \text{ and } LAI \neq 0 \\ 0 & \text{for } T \leq t_{snow} \text{ and } LAI = 0 \end{cases}$$

acc_{ground} = Accumulation ground [mm]

acc_{canopy} = Accumulation canopy [mm]

p = Precepitation [mm]

I = Interception [mm]

T = Temperature [°C]

t_{snow} = Snow fall temperature [°C]

LAI = Leaf area index [-]

$$p_{ground} = \begin{cases} p \times (1 - cc) & \text{for } T \geq t_{snow} \text{ and } LAI \neq 0 \\ p & \text{for } T \geq T_{snow} \text{ and } LAI = 0 \end{cases} \tag{2.10}$$

$$p_{canopy} = \begin{cases} p \times cc & \text{for } T \geq T_{snow} \text{ and } LAI \neq 0 \\ 0 & \text{for } T \geq T_{snow} \text{ and } LAI = 0 \end{cases}$$

p_{ground} = Rain reaching the ground-layer [mm]

p_{canopy} = Rain intercepted in the canopy [mm]

p = Precepitation [mm]

cc = Canopy Coverage [-]

T = Temperature [°C]

T_{snow} = Snow fall temperature [°C]

LAI = Leaf area index [-]

2.5.12 Potential Melt

Potential melt is calculated using the degree-day method. Melt occurs when temperatures are above the melting point. Then, a defined amount of SWE melts per degree above melting temperature per day (Formula (2.11)).

$$M_{canopy,pot} = \begin{cases} DDF_{canopy} \times T & \text{for } T > T_{melt} \\ 0 & \text{for } T \leq T_{melt} \end{cases} \tag{2.11}$$

$$M_{ground,pot} = \begin{cases} DDF_{ground} \times T & \text{for } T > T_{melt} \\ 0 & \text{for } T \leq T_{melt} \end{cases}$$

$M_{canopy,pot}$ = Potential melt in the canopy layer [mm]

$M_{ground,pot}$ = Potential melt on ground surface [mm]

DDF_{ground} = DDF for ground layer [mm $^{\circ}C^{-1}$ d^{-1}]

DDF_{canopy} = DDF for canopy layer [mm $^{\circ}C^{-1}$ d^{-1}]

T = Temperature [°C]

T_{melt} = Melting-temperature [°C]

2.5.13 Potential Rain Melt

The module is equipped with equations to calculate rain on snow melt. Liquid precipitation, divided in the accumulation routine, leads to additional snow melting in the canopy and ground layers. The amount of rain melting can be determined by calculating the amount of energy released by rain warmer than melting temperature, using the heat capacity of liquid water. Then the amount of rain melt is equal to the energy released, divided by the melt enthalpy of solid water (Formula (2.12)).

$$M_{canopy,pot} = p_{canopy} \times T \times C \times H_{melt}^{-1} \tag{2.12}$$

$$M_{ground,pot} = \begin{cases} p_{ground} \times T \times C \times H_{melt}^{-1} & \text{for } SWE_{canopy,0} > 0 \\ (p_{ground} + p_{canopy}) \times T \times C \times H_{melt}^{-1} & \text{for } SWE_{canopy,0} = 0 \end{cases}$$

$M_{canopy,pot,rain}$ = Potential rain melt in the canopy layer [mm]

$M_{ground,pot,rain}$ = Potential rain melt on ground surface [mm]

$SWE_{canopy,0}$ = SWE in canopy at the beginning of the time-step [mm]

p_{ground} = Rain reaching the ground-layer [mm]

p_{canopy} = Rain intercepted in the canopy [mm]

T = Temperature [°C]

C = Heat capacity of liquid water = 4190 J kg^{-1}

H_{melt} = Melt enthalpy of ice = 334 000 J kg^{-1}

2.5.14 Potential Sublimation

A routine was developed to calculate a sublimation value. Therefore, the potential evaporation input is used. Base sublimation is given as the product of the potential evapotranspiration value and the ratio of evaporation- to sublimation-enthalpy (Formula (2.13) and (2.14)). Sublimation below canopy is assumed to be inversly proportional to the LAI for three reasons: First the LAI influences the amount of radiation reaching the ground layer and therefore reducing the amount of energy available for sublimation on the ground snow layer. Second, the sublimating canopy snow increases humidity lowering the sublimation on the ground. Third, windspeed is reduced on the ground surface and therefore lessens sublimation on the ground layer even further. To put those effects in a simple formula, inverse proportionality of LAI and ground sublimation suggests itself.

The sublimation on the ground layer equals the unmodified sublimation value when no canopy is present. In canopy sublimation losses of SWE are estimated as the product of LAI and base sublimation. This is due to the increased surface area (which is proportional to the LAI) of the snow cover in canopy. This is summarized in Formula (2.15).

$$H_{sub} = H_{melt} \times H_{evap} \tag{2.13}$$

H_{sub} = Sublimation enthalpy [J kg^{-1}]

H_{melt} = Melt enthalpy [J kg^{-1}] H_{evap} = Evaporation enthalpy [J kg^{-1}]

$$S = ET \times ts \times \frac{H_{evap}}{H_{sub}} \tag{2.14}$$

S = Potential sublimation [mm]

ET = Potential evapotranpiration [mm d^{-1}]

ts = Time step [d]

H_{evap} = Evaporation enthalpy [J kg^{-1}]

H_{sub} = Sublimation enthalpy [J kg^{-1}]

$$S_{ground} = \begin{cases} \frac{S}{LAI \times cc} & \text{for } LAI > 0 \text{ and } cc > 0 \\ S & \text{for } LAI = 0 \text{ for } cc = 0 \end{cases} \tag{2.15}$$

$$S_{canopy} = \begin{cases} S \times LAI \times cc & \text{for } LAI > 0 \text{ and } cc > 0 \\ 0 & \text{for } LAI = 0 \text{ or } cc = 0 \end{cases}$$

S_{ground} = Potential sublimation ground layer [mm]

S_{canopy} = Potential sublimation canopy layer [mm]

S = Potential sublimation [mm]

cc = Canopy Coverage [-]

LAI = Leaf Area Index [-]

2.5.15 Calculating actual SWE

The heart of the model is the calc_swe routine. It determines actual SWE values from potential melt, rain melt and sublimation. The algorithm for canopy- and ground layer follows the same scheme:

1. Add accumulation, to the initial SWE value: Formula (2.16)
2. Subtract sublimation: Formula (2.17)
3. Subtract melt: Formula(2.17)
4. Subtract rain melt: Formula (2.17)

$$SWE_1 = SWE_0 + acc \tag{2.16}$$

SWE_1 SWE after the time step [mm]

SWE_0 SWE before the time step [mm]

acc = Accumulation ground or canopy [mm]

$$SWE_1 = \begin{cases} 0 & \text{for } SWE_0 < x_{pot} \\ SWE_0 - x_{pot} & \text{for } SWE_0 \geq x_{pot} \end{cases} \tag{2.17}$$

$$x_{real} = \begin{cases} x_{pot} - SWE_0 & \text{for } SWE_0 < x_{pot} \\ x_{pot} & \text{for } SWE_0 \geq x_{pot} \end{cases}$$

SWE_1 = SWE after the time step [mm]

SWE_0 = SWE before the time step [mm]

x_{pot} = Potential value for sublimation, melt or rain melt [mm]

x_{real} = Actual sublimation, melt or rain melt [mm]

2.5.16 Unloading

After sublimation and melt processes are dealt with, unloading can be calculated. Unloading is controlled by an unloading factor. It gives the fraction of snow unloaded from initial SWE from the canopy to the ground layer. This equation (Formula (2.18)) is similar to the exponential decay widely used in different snow modules (J. Pomeroy et al. 1998) (Yang, Endreny, and Nowak 2011) (Mahat and Tarboton 2014).

$$ul = SWE_1 \times uf \times ts \tag{2.18}$$

ul = Unloaded snow [mm]

SWE_1 = SWE after the time step [mm]

uf = Unloading factor [-]

ts = Time step [d]

2.5.17 Liquid Water

The liquid water routine consists of two parts. First the liquid water content of the canopy layer is calculated. Therefore, intercepted rain, melt and rain melt are added to the initial liquid water content. This happens when (1) there is snow on canopy and (2) when temperature is above freezing temperature. When the temperature drops below freezing temperature, the liquid storage is frozen and adds to the canopy SWE at a rate dependent on the base DDF and the refreezing rate. If liquid storage exceeds the storage capacity the excess water goes to dripping and canopy liquid content is set to maximal storage capacity. The flowchart (Figure 2) visualizes the process. Calculation details are shown in the Formulas (2.19) - (2.23). The second part is the ground layer liquid water calculation (Figure 3). It follows the structure of the canopy layer calculation. What's different is that dripping from canopy adds to the ground snow layer, and exiting water is diverted to outflow (compare Formula (2.24) - (2.28)).

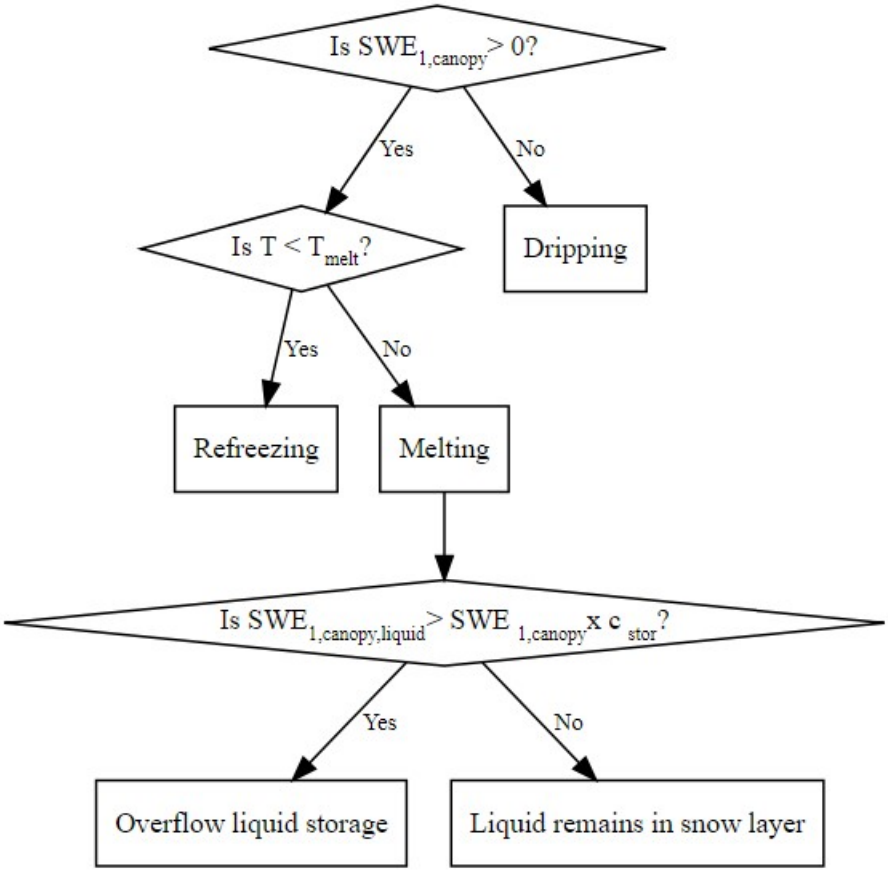

Figure 2: Workflow of the canopy liquid water routine.

Dripping (2.19)

$$D = SWE_{0,\text{canopy,liquid}} + M_{\text{canopy,rain}} + M_{canopy} + I$$

$$SWE_{2,\text{canopy}} = SWE_{1,\text{canopy}}$$

$$SWE_{2,\text{canopy,liquid}} = 0$$

Refreezing (2.20)

$$D = 0$$

$$SWE_{2,\text{canopy}} = \begin{cases} SWE_{1,\text{canopy}} + c_{ref} \times DDF_{base} \times ts & \text{for } SWE_{2,\text{canopy,liquid}} > c_{ref} \times DDF \times ts \\ SWE_{1,\text{canopy}} + SWE_{1,\text{canopy,liquid}} & \text{for } SWE_{2,\text{canopy,liquid}} \leq c_{ref} \times DDF \times ts \end{cases}$$

$$SWE_{2,\text{canopy,liquid}} = \begin{cases} SWE_{1,\text{canopy,liquid}} - c_{ref} \times DDF_{base} \times ts & \text{for } SWE_{2,\text{canopy,liquid}} > c_{ref} \times DDF \times ts \\ 0 & \text{for } SWE_{2,\text{canopy,liquid}} \leq c_{ref} \times DDF \times ts \end{cases}$$

Melt (2.21)

$$SWE_{1,\text{canopy,liquid}} = M_{\text{canopy,rain}} + M_{canopy} + I$$

Overflow liquid storage (2.22)

$$D = SWE_{1,\text{canopy,liquid}} - SWE_{1,\text{canopy}} \times c_{\text{stor}}$$

$$SWE_{2,\text{canopy}} = SWE_{1,\text{canopy}}$$

$$SWE_{2,\text{canopy,liquid}} = SWE_{1,\text{canopy}} \times c_{\text{stor}}$$

Liquid remains in snow layer (2.23)

$$D = 0$$

$$SWE_{2,\text{canopy}} = SWE_{1,\text{canopy}}$$

$$SWE_{2,\text{canopy,liquid}} = SWE_{2,\text{canopy,liquid}}$$

D = Dripping [mm]

$SWE_{0,canopy,liquid}$ = Initial liquid water content in canopy [mm]

$SWE_{1,canopy}$ = SWE in canopy before liquid-content calculations [mm]

$SWE_{2,canopy}$ = SWE in canopy after liquid-content calculations [mm]

$SWE_{1,canopy,liquid}$ = Liquid water in canopy after adding melt, rain melt and intercepted rain [mm]

$SWE_{2,canopy,liquid}$ = Liquid water in canopy after liquid water calculations [mm]

M_{canopy} = Real melt in canopy [mm]

$M_{canopy,rain}$ = Rain melt in canopy [mm]

I = Intercepted rain in canopy [mm]

DDF_{base} = Fixed part of the DDF [mm °C^{-1} d^{-1}]

ts = Time step [d]

c_{stor} = Storage coefficient in fraction of SWE [-]

c_{ref} = Refreezing coefficient [mm/d]

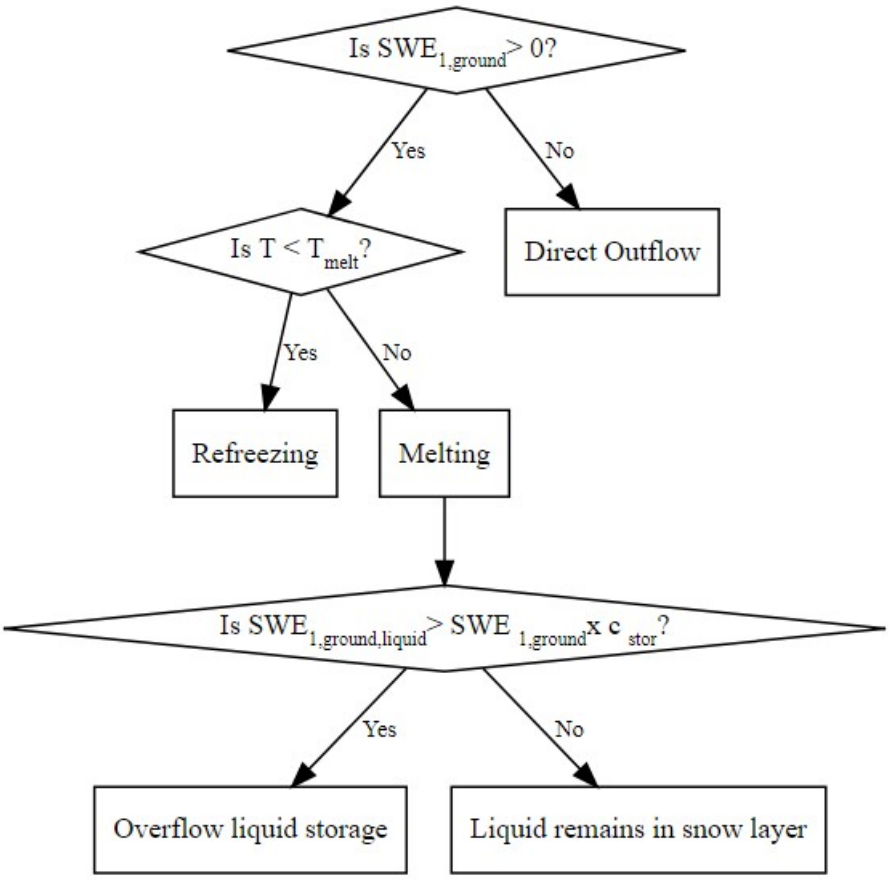

Figure 3: Flowchart of the ground-layer's liquid water routine.

Direct outflow (2.24)

$$O = SWE_{0,\text{ground,liquid}} + M_{\text{ground, rain}} + M_{ground} + P_{ground} + D$$

$$SWE_{2,\text{ground}} = SWE_{1,\text{ground}}$$

$$SWE_{2,\text{ground,liquid}} = 0$$

Refreezing (2.25)

$$O = 0$$

$$SWE_{2,\text{ground}} = \begin{cases} SWE_{1,\text{ground}} + c_{ref} \times DDF_{base} \times ts & \text{for } SWE_{2,\text{ground,liquid}} > c_{ref} \times DDF \times ts \\ SWE_{1,\text{ground}} + SWE_{1,\text{ground,liquid}} & \text{for } SWE_{2,\text{ground,liquid}} \leq c_{ref} \times DDF \times ts \end{cases}$$

$$SWE_{2,\text{ground,liquid}} = \begin{cases} SWE_{1,\text{ground,liquid}} - c_{ref} \times DDF_{base} \times ts & \text{for } SWE_{2,\text{ground,liquid}} > c_{ref} \times DDF \times ts \\ 0 & \text{for } SWE_{2,\text{ground,liquid}} \leq c_{ref} \times DDF \times ts \end{cases}$$

Melt (2.26)

$$SWE_{1,\text{ground,liquid}} = M_{\text{ground,rain}} + M_{ground} + P_{ground} + D$$

Overflow liquid storage (2.27)

$$O = SWE_{1,\text{ground,liquid}} - SWE_{1,\text{ground}} \times c_{\text{stor}}$$

$$SWE_{2,\text{ground}} = SWE_{1,\text{ground}}$$

$$SWE_{2,\text{ground,liquid}} = SWE_{1,\text{ground}} \times c_{\text{stor}}$$

Liquid remains in snow layer (2.28)

$$O = 0$$

$$SWE_{2,\text{ground}} = SWE_{1,\text{ground}}$$

$$SWE_{2,\text{ground,liquid}} = SWE_{2,\text{ground,liquid}}$$

O = Outflow to the soil surface [mm]

$SWE_{0,ground,liquid}$ = Initial liquid water in ground snow layer [mm]

$SWE_{1,ground}$ = SWE in ground snow layer before liquid-content calculations [mm]

$SWE_{2,ground}$ = SWE in ground snow layer after liquid-content calculations [mm]

$SWE_{1,ground,liquid}$ = Water in ground layer after melt, rain melt and interception [mm]

$SWE_{2,ground,liquid}$ = Water in ground layer after liquid water calculations [mm]

M_{ground} = Real melt in ground snow layer [mm]

$M_{ground,rain}$ = Rain melt in ground snow layer [mm]

P_ground = Rain on ground [mm]

D = Dripping from Canopy [mm]

DDF_{base} = Fixed part of the DDF [mm °C^{-1} d^{-1}] (Hock 1999)

ts = Time step [d]

c_{stor} = Storage coefficient in fraction of SWE [-]

c_{ref} = Refreezing coefficient [mm/d]

2.6 Goodness of Fit Measures

To quantify the model error different "goodness of fit" measures are available. The decision was made to integrate Mean Absolute Error (MAE) and Root Mean Squared Error (RMSE). Both are used to quantify the accuracy of results in the work of Geissler, Rathmann, and Weiler (2023). To provide a comprehensive assessment of model performance, capturing both the magnitude and timing of events the Kling Gupta Efficiency (KGE, Formula (2.29), Gupta et al. (2009)) measure was calculated to compare ΔSnow and model data. KGE captures correlation, bias, and variability and is therefore better suited to describe the model efficiency than MEA or RMSE alone.

$$\mathrm{KGE} = 1 - \sqrt{(r-1)^2 + \left(\frac{\sigma_{sim}}{\sigma_{obs}} - 1\right)^2 + \left(\frac{\mu_{sim}}{\mu_{obs}} - 1\right)^2} \tag{2.29}$$

r = Linear correlation between observations and simulations

σ_{obs} = Standard deviation in observations

σ_{sim} = Standard deviation in simulations

μ_{obs} = Observation mean

μ_{sim} = Simulation mean

2.7 Parameter Configuration and Model Comparison

Parameters for modelling clusters A-D were set manually. This was done following these guidelines:

- Refreezing rate was set to 1, storage coefficient to 0.08 (roughly following maximum liquid water content of 10% after Techel and Pielmeier (2011), mimicking the Nordic HBV settings (Saelthun 1996)).
- The unloading factor was set to 0.1 for all clusters.
- Latitude, elevation, slope and aspect were taken as mean values from Geissler, Rathmann, and Weiler (2023).
- LAI and canopy coverage were obtained from Geissler, Rathmann, and Weiler (2023) for all 4 clusters.
- Shade was set to zero for forested and open-exposed areas. The open-shaded cluster was modelled with a shading value of 0.9 due to shading of the surrounding forest. Shade for the Open intermediate cluster was set to 0.5. The cluster was described as areas neighbouring forest in eastern or western directions. Accordingly direct sunlight reaches those areas in 50% of the whole sunshine duration.
- DDF was set higher in forested clusters (cluster D), or clusters surrounded by forest (cluster A). This was done, to take amplified long-wave radiation in forested areas into account. DDF is usually lower for clusters with less trees (cluster B, C).
- Snowfall temperature was adjusted to be lower in forested clusters. This was done to model long-wave radiation and reduced heat-flux effects.

To ascertain an input data resolution that yields reasonable model outcomes, the model was evaluated using both daily and hourly temperature inputs. All four clusters were simulated, each cluster with an individual parameter set. Time step was equally set for all simulations to 60 minutes to ensure fast calculation and sufficient precision of the model output at the same time. Model output was compared to the ΔSnow time series from Geissler, Rathmann, and Weiler (2023). Therefore, an error margin was added to the Geissler-SWE-data. It was calculated multiplying the percent mean RMSE to the Geissler model output. Manual SWE measurements also provided by Geissler, Rathmann, and Weiler (2023) were used for validating model results. For each sample day the standard deviation was calculated for all measurement assigned to one cluster.

After a visual inspection of the model's ground layer SWE output snowfall temperature was farther adjusted to reach a good fit of accumulation intervals and magnitudes. The same was applied to the DDF for melt processes. The model was adjusted to fit the winter season 2021-2022 (2021-11-15 until 2022-05-01). Then the same input values were used to model the 2020-2021 (2020-11-15 until 2021-05-14) winter season without further calibration.

2.8 Model Output Post-Processing

For creating graphs and tables, data were read, aggregated and evaluated with the tidyverse-package (R 4.2.0, tidyverse-package). Plots were made with ggplot, also taken from the tidyverse-package. Plot-arrangement was done with patchwork (R 4.2.0, Pedersen (2020)). Tables were created with kableExtra (R 4.2.0, Zhu (2021)).

2.9 Creating Accumulation and Ablation Curves

Accumulation and ablation curves were created with code available in the markdown file attached to this thesis. The algorithm detects increases or decreases in ground SWE (liquid water content included) for each time step. Values were plotted cumulatively.

2.10 Canopy Layer Evaluation

To assess the precision of the canopy layer routine of the snow model, the following solution was found. The test-area has been photographed every 6 hours by various SnoMoS. The data was obtained from Geissler, Rathmann, and Weiler (2023). Two SnoMoS were identified (Figure 4), one facing a south-, the other a north-canopy-edge. Time series were created containing boolean values for snow-cover in canopy by visual inspection of the images. Those were then compared to the model forested cluster (hourly temperature input) canopy SWE output. Images were screened manually for snow in canopy following these guidelines:

- Snowfall even during night time is easily visible in the pictures, because the flashlight of the camera is reflected by snow flakes. The flash does not reach the canopy edges properly. Therefore determination of snow in canopy during night is difficult in foggy conditions. It is assumed that snow in canopy is present when snow is falling.

- Especially during night time branches seem white due to the flash, rime ice or hoarfrost. This is not counted as snow in canopy layer.
- If snow or no snow in canopy cannot be clearly distinguished, no snow is assumed.

The amount of hours when snow in the canopy was present in both the images and the model results were counted. The results were divided by the total amount of snow-hours in the pictures. This was done for the north and south facing canopy edges for a time period in between 2021-11-01 00:00:00 and 2022-05-01 00:00:00.

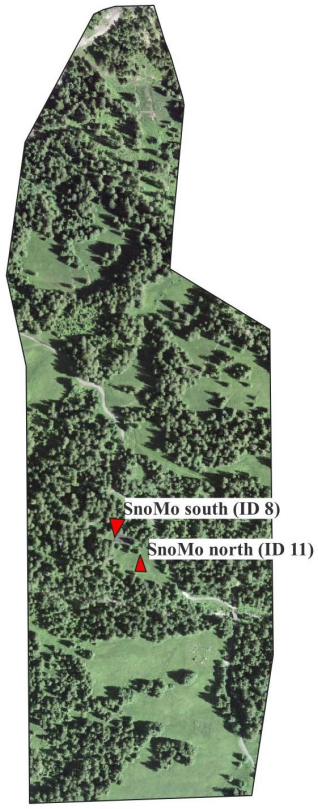

Figure 4: Position of the SnoMoS used for evalutating the canopy snow layer. Angle of sight is indicated by the red triangle.

3 Results

3.1 Model Parameters, Resolution and Performance

To match the ΔSnow SWE-time-series 2021-2022 parameters were adjusted accordingly. Table 5 shows the adjusted parameters used for the individual model runs. Snowfall temperature is lowest in the forested cluster (0.1 °C). The other clusters show higher thresholds between 0.4 and 0.7 °C. The base-DDF is distributed between 1.2 and 1.4 mm°C^{-1}d^{-1}.

Table 5: Input data for modelling clusters A-D with daily and hourly temperature data.

Model Variable	Open-shaded	Open-exposed	Open-intermediate	Forested	Unit
storage_coef	0.08	0.08	0.08	0.08	-
unloading_factor	0.10	0.10	0.10	0.10	-
canopy_coverage	0.20	0.40	0.30	0.80	-
ddf	1.20	1.20	1.30	1.40	mm/°C/day
t_snowfall	0.70	0.40	0.50	0.10	°C
shade	0.90	0.00	0.50	0.00	-
lai	4.00	4.00	4.00	4.50	-
refreezing_rate	1.00	1.00	1.00	1.00	-
elev	1200.00	1200.00	1200.00	1200.00	MSL
lat	47.00	47.00	47.00	47.00	degree
slope	15.00	15.00	15.00	15.00	degree
aspect	250.00	250.00	250.00	250.00	degree
station_exposure	4.00	4.00	4.00	4.00	-

3.1.1 Calibration Season 2021 - 2022

For the 2021/22 winter season all SWE time-series closely follow the ΔSnow-SWE by Geissler, Rathmann, and Weiler (2023) (Figure 5). This indicates that the model is generally capturing the overall trend of snow accumulation and ablation. However, the model appears to encounter challenges in balancing snow accumulation and ablation processes. Distinct variations in both accumulation and ablation between midwinter and spring are noticeable. The model shows discrepancies in capturing the correct intensity of these processes.

Noticeable differences between model and reference data are visible in the mid winter melt event in late December to early January. In cluster B and D (open exposed and forested) its magnitude is underestimated. Melt rates are to low to match the ΔSnow time series. The resulting error in SWE is about 50 mm. For the open exposed site deficits in accumulation, predicted by the model, are closing this gap in the later season. The same is true for the forested cluster hourly temperature

input time series. Modelling with daily temperature leads to a bigger gap between model output and the ΔSnow data in the forested cluster.

Clusters A-C exhibit disparities between the simulated ΔSnow values and the model output. In both cases, the April melt rates are underestimated. However, the model adequately captures the melt rates in March. The model fails to capture the abrupt shifts in melt rates, resulting in a delayed prediction of the end of snow cover. This lag amounts to less than one week.

The ΔSnow time series exhibits two phases of static SWE conditions. The first is located in December, the second in late March until mid April. The model shows a reduction of SWE in those phases for all clusters.

Utilizing hourly temperature input appears to yield a slight enhancement in model output. Observable disparities in the individual cluster's time series are evident. In the open shaded cluster, a substantial accumulation event in early February results in differences of up to 50 mm in SWE model output due to the utilization of hourly temperature data. Conversely, the forested cluster exhibits a contrasting behaviour. In this case, accumulation events are overestimated by the model that calculates with daily temperature input. This discrepancy is notable in the accumulation events at the outset of February. In the open exposed and open intermediate clusters, both hourly and daily temperature input data lead to negligible differences in model output.

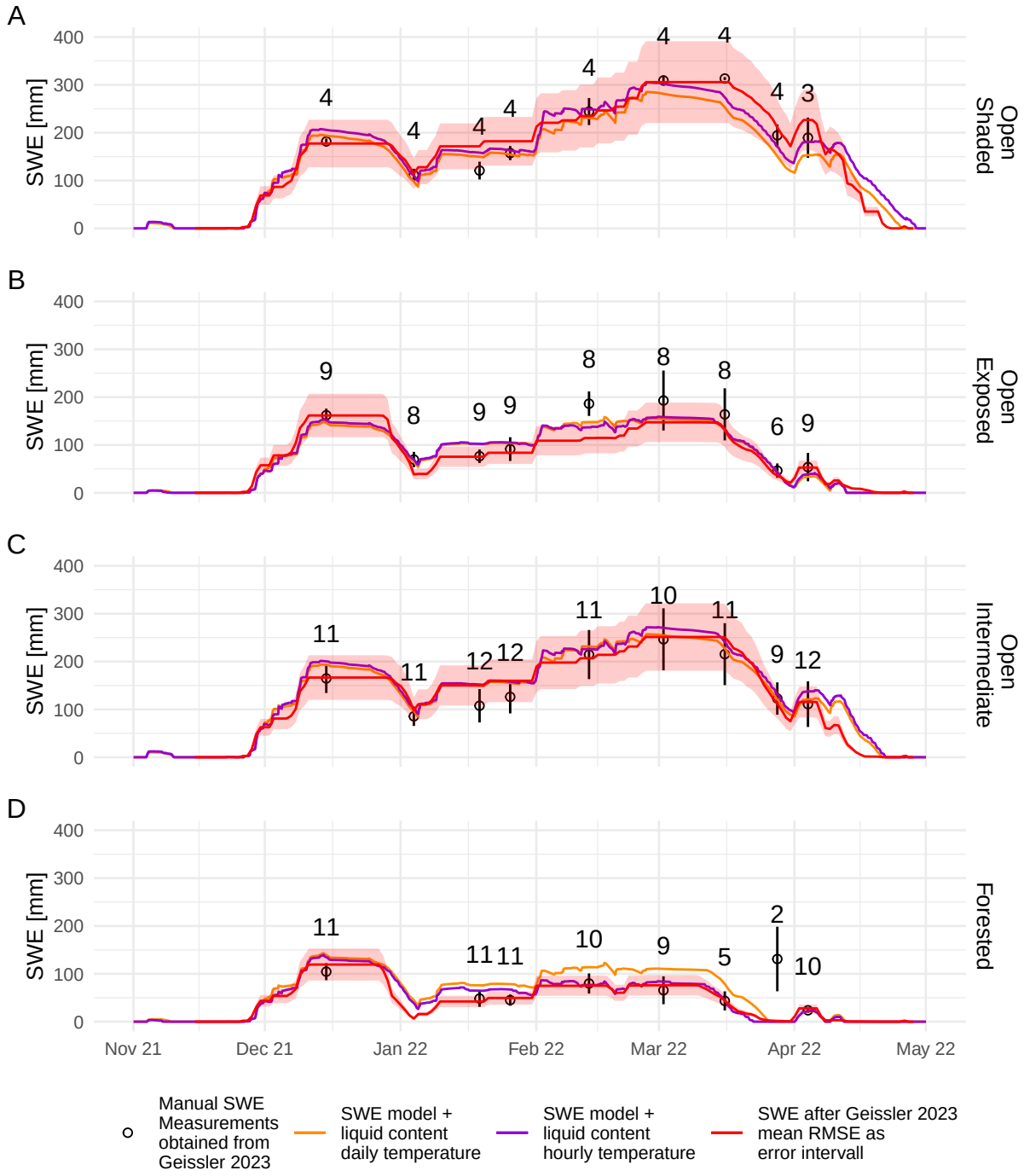

Figure 5: Plots for model runs 2021/22 with mean daily temperature (orange) and hourly temperature (violet) for clusters A-D. Shown is ground layer SWE (liquid water in the snow-cover adds to SWE). The red line marks the SWE modelled by Geissler 2023 with RSME (28%) multiplied to each value to create the red error band. Count, mean and standard deviation are plotted for manual SWE measurements in black. Model parameters were adjusted to fit the ΔSnow SWE data.

3.1.2 Validation Season 2020 - 2021

To gain insights into the consistency of model outcomes, a second season was simulated for evaluation purposes. The simulated time-series closely align with both the ΔSnow model output from Geissler, Rathmann, and Weiler (2023) and the manually collected SWE measurements, with a few exceptions (Figure 6).

Two melt events were incorrectly predicted by the model. One in the beginning of December and a second in late January until early February. In both events model predictions are above the amount of melt indicated by the ΔSnow time series. This is ture for all clusters. The largest deviations between model results and observed data are observed in the open shaded cluster. In this cluster, the melt event at the end of February leads to an SWE deficit of up to 100 mm in both hourly and daily temperature simulations.

In contrast to the last observation a melt event is present in the Geissler, Rathmann, and Weiler (2023) ΔSnow data in early April which is not accounted for in the model results for all but the forested cluster.

Furthermore snow falling during late January is not simulated well by the model. Snowfall is overestimated by the model when referring to the ΔSnow time series. However the model results lie well within reach of the manual snow measurements error margins.

Discrepancies between hourly and daily temperature input are noticeable in all clusters except the open intermediate one. In the remaining three clusters the model's SWE differs from the ΔSnow data during the accumulation period in late January. The resulting error is carried through the rest of the season. In the open shaded cluster hourly temperature modelling leads to higher SWE. The opposite is true for the open exposed and the forested cluster.

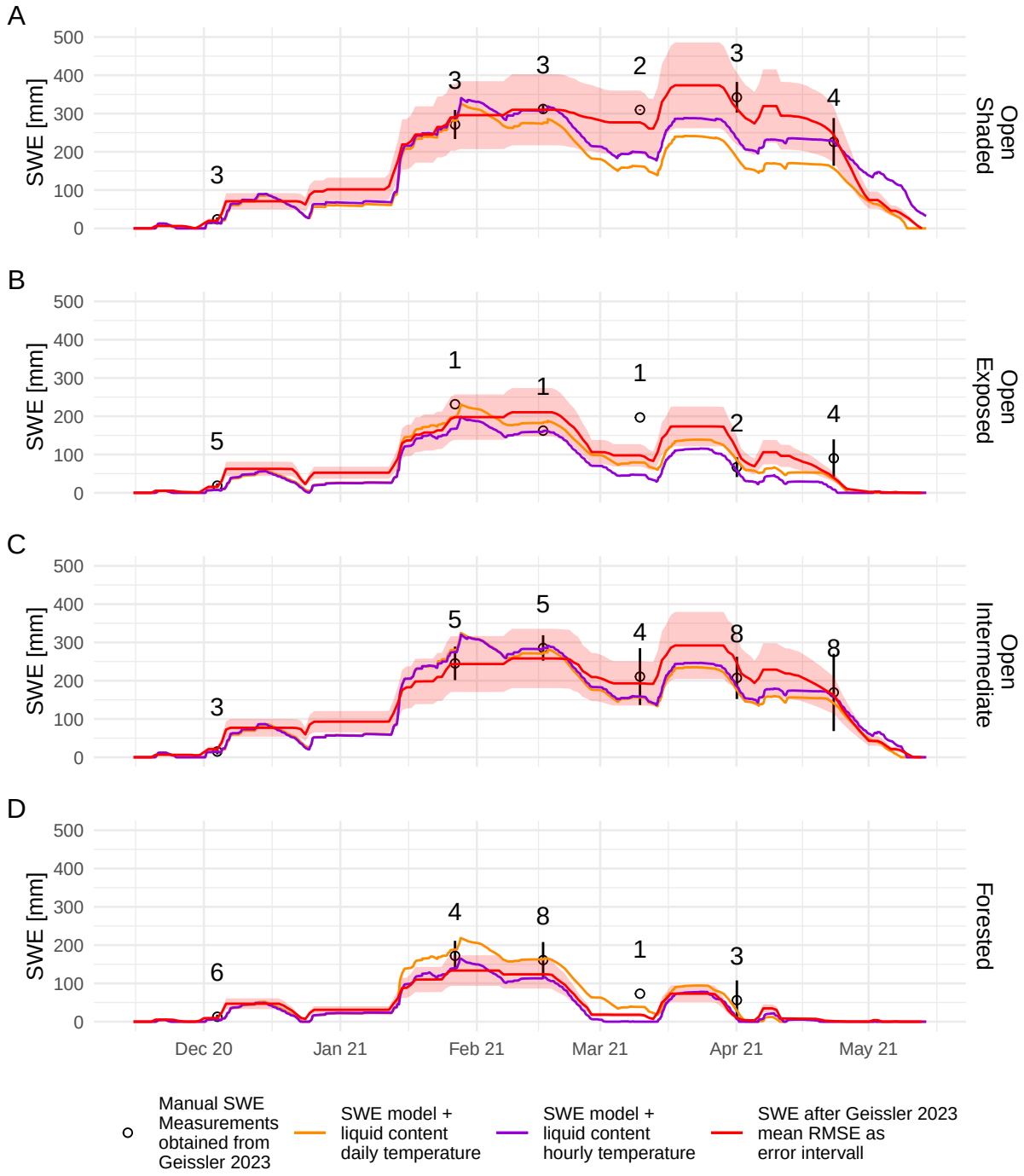

Figure 6: Plots for model runs winter 2020/21 with mean daily temperature (orange) and hourly temperature (violet) for clusters A-D. Shown is ground layer SWE (liquid water in the snow-cover addes to SWE). The red line marks the SWE modelled by Geissler 2023 with NRSME (30%) multiplied to each value to create the red error band. Count, mean and standard deviation are plotted for manual SWE measurements in black. No futher adjustment to the model parameters was made to provide validation for the 2021/22 model configuration.

3.2 Quantitative Model Evaluation

To quantify the model error different "goodness of fit" measures are available. The decision was made to integrate MAE and RMSE. Both are used to quantify the accuracy of results in the work of Geissler, Rathmann, and Weiler (2023). To provide a comprehensive assessment of model performance, capturing both the magnitude and timing of events the KGE measure was calculated to compare

*Delta*Snow and model data. KGE captures correlation, bias, and variability of time-series and is therefore better suited to describe the model efficiency than MEA or RMSE alone. A list of the three named measures comparing all model runs to the

*Delta*Snow time series is shown in Table 6.

Model performance is better for the calibration season 2021/22 than for validation in 2020/21. The overall pattern is that hourly temperature input leads to similar or better model results compared to the daily temperature input. The exception is the 2020/21 open-exposed simulation. For this cluster a model based on daily temperature performs slightly better. The highest difference between daily and hourly temperature input can be seen in the forested cluster. Hourly temperature input almost doubles the KGE. RMSE and MAE are halved.

Table 6: Comparison of the Geissler 2023 ΔSnow data and the models ground-layer SWE (liquid content included) with KGE, RMSE and MAE.

	Daily Temperature			Hourly Temperature		
Cluster	KGE	RMSE	MAE	KGE	RMSE	MAE
Season 2020/21						
Open shaded	0.64	75.43	55.46	0.80	49.62	38.02
Open exposed	0.82	24.03	20.07	0.62	39.06	31.57
Open intermediate	0.87	38.79	31.43	0.90	33.98	28.26
Forested	0.46	27.20	18.65	0.87	10.78	8.35
Season 2021/22						
Open shaded	0.83	30.24	22.65	0.91	24.91	19.77
Open exposed	0.92	18.26	14.30	0.91	16.53	13.33
Open intermediate	0.94	17.63	12.22	0.90	21.70	15.78
Forested	0.52	24.86	19.95	0.84	11.94	8.24

3.3 Accumulation

The model outcomes exhibit a notable sensitivity to the selected threshold temperature (refer to Figure 13 in Appendix). This threshold temperature stands as the sole parameter that affects variations in SWE. To assess this relatively straightforward algorithm, all accumulation events are cumulatively aggregated, with liquid content contributing to SWE. The results are illustrated in Figure 7 for all the model runs previously described. Across all plots, the model consistently overestimates accumulation quantities when compared against the data from Geissler, Rathmann, and Weiler (2023).

This pattern remains relatively consistent across all clusters and temperature input simulations. Five primary accumulation events can be identified:

The initial accumulation happens in late November, marking the onset of the snowfall period. This event concludes during the second week of December, leading to discernible differences in SWE across all clusters except the open exposed one. The second event occurs at the beginning of January, resulting in an increase of the modelled SWE levels. Once again, the open exposed cluster stands as the exception. Toward the end of January, the ΔSnow model indicates a steady increase in SWE, a trend not mirrored by the model data. Around the beginning of February, a third high magnitude accumulation event emerges in the model's SWE time-series. Absent in the Geissler, Rathmann, and Weiler (2023) model data, this event bridges the SWE disparity. Distributed over the entirety of February, the fourth accumulation phase begins. Persistent model overestimation leads to deficits ranging from 50 to 200 mm in SWE compared to the ΔSnow model time series. The beginning of April sees an accumulation event that appears to be well-matched by the model data.

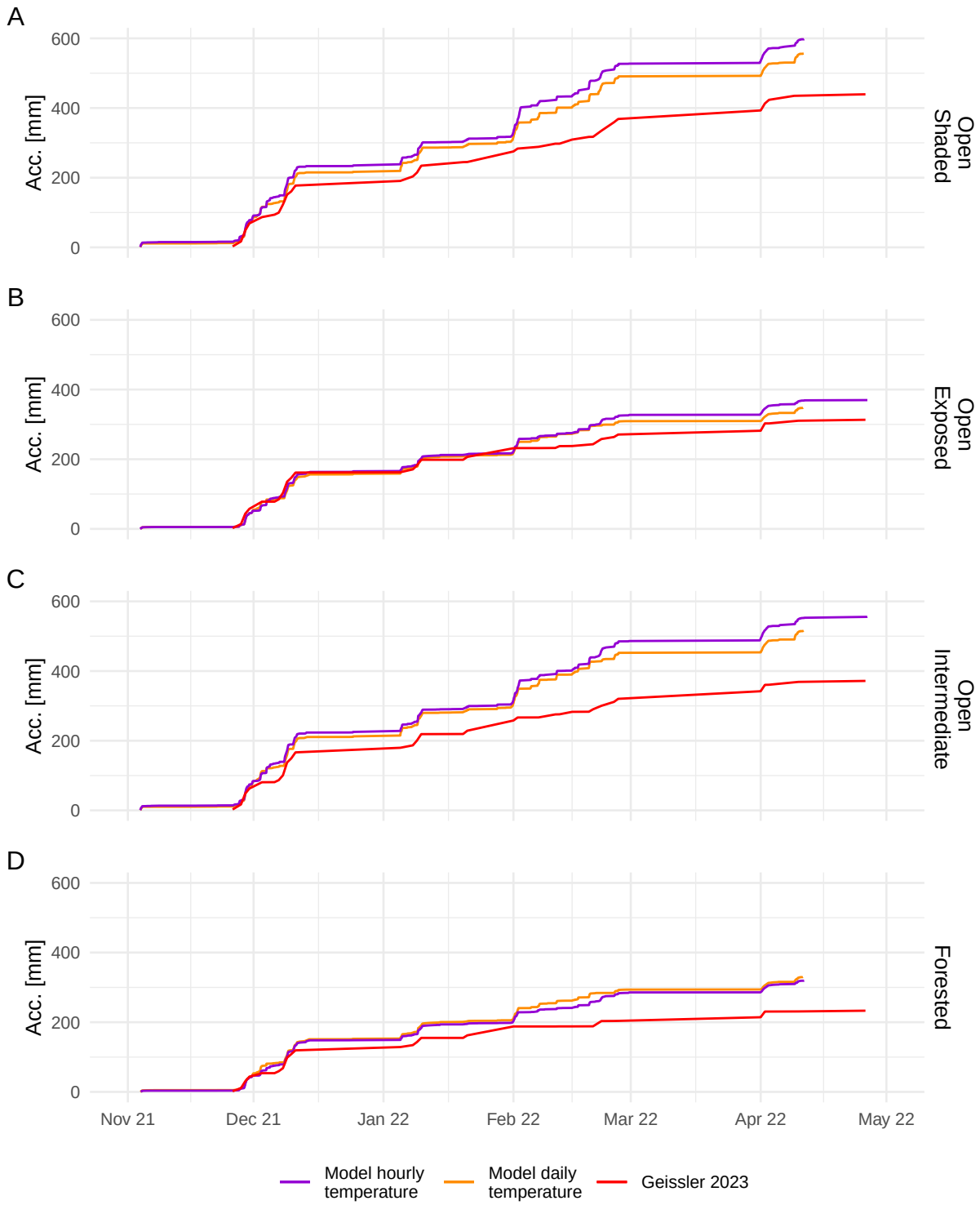

Figure 7: Plots for 2021-2022 accumulation processes with mean daily temperature (orange) and hourly temperature (violet) SWE simulations 2021-2022 for cluster A-D. The red line marks the cumulative gains in SWE modelled by Geissler 2023.

3.4 Ablation

In contrast to the accumulation processes, various model routines influence ablation processes. Temperature- and rain-induced melting ultimately result in outflows, reducing the SWE, while sublimation directly removes water from the SWE and releases it into the air. The combined effect of these processes, accumulated over the 2021/22 season, is depicted in Figure 8. Notably, all model runs tend to overestimate ablation.

The initial decrease in snow-cover SWE becomes apparent by the end of December in the ΔSnow graph from Geissler, Rathmann, and Weiler (2023). However, all model curves show ablation occurring before this date. The discrepancy between the model and reference data varies from nearly zero (exposed (B) and forested (D) clusters) to approximately 50 mm SWE (shaded (A) and intermediate (C) clusters).

Between late December and mid-March, the ΔSnow data for clusters 1-3 (A-C) do not indicate any significant ablation. However, in the forested cluster, the data suggests a minor melting event in mid-February. This leads to an expanding difference between the reference and model data, ranging from approximately 100 mm (for the exposed and forested clusters) to around 200 mm (for the shaded and intermediate clusters) of SWE. Ablation rates appear to align more closely in late March and early April.

Notably, the conclusion of the snow season is predicted with reasonable accuracy across the clusters, generally falling within a margin of about one week. It's worth highlighting that, in the forested cluster, the model anticipates the end of the snow season to be about two weeks earlier than the observed data.

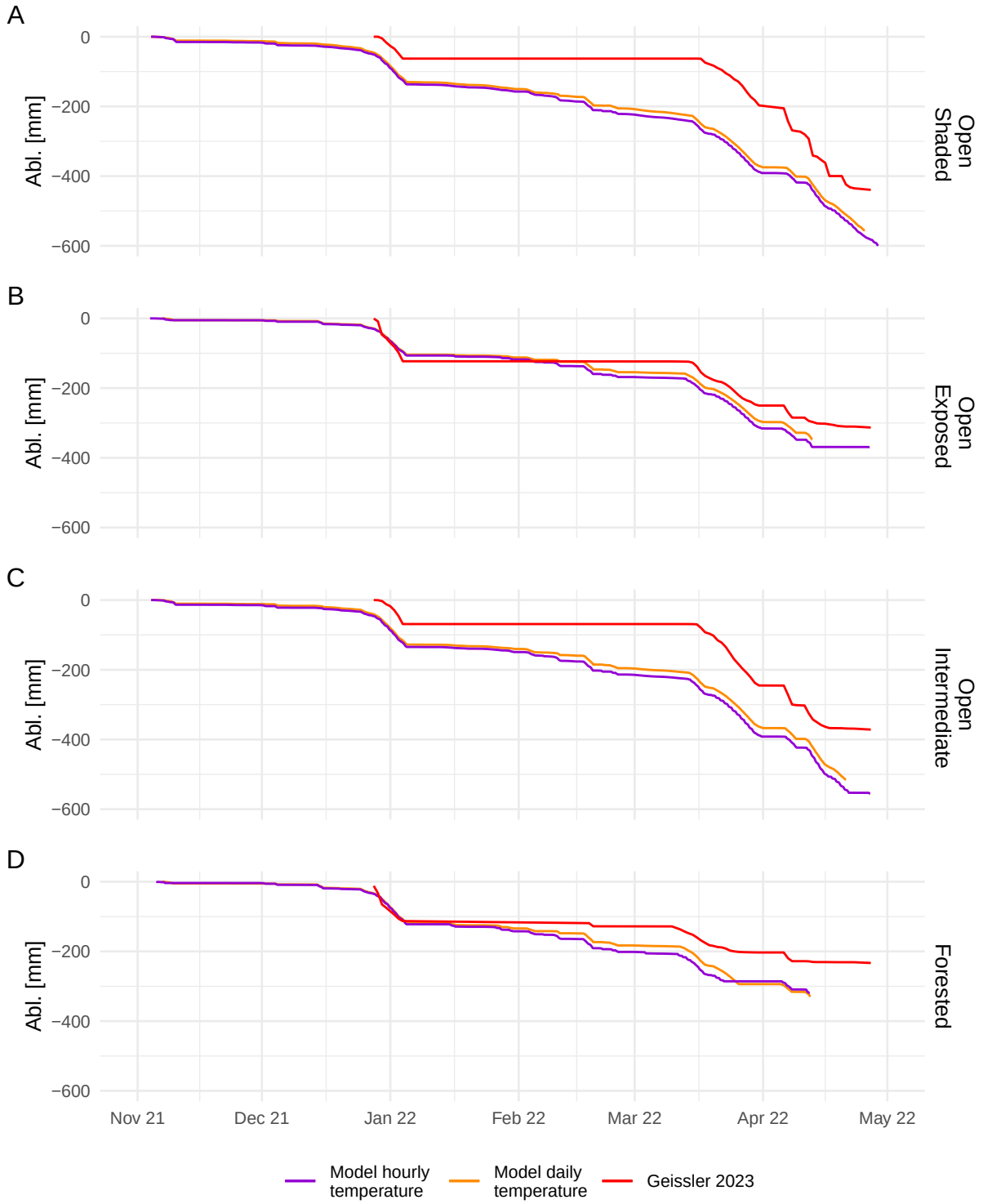

Figure 8: Plots for ablation processes with mean daily temperature (orange) and hourly temperature (violet) SWE simulations 2021-2022 for clusters A-D. Red lines indicated the cumulated losses in SWE from the ΔSnow time series obtained from the Geissler 2023.

3.5 Sublimation

Evaluating sublimation on a daily basis can prove challenging. This is primarily caused by a lack of reference data. Data for comparison are available for whole seasons. Therefore, the model data was compared to seasonal evaporation values from literature. Table 7 gives an overview on seasonal sublimation values of described model runs. Sublimation is split between ground and canopy layer for hourly- and daily-input model results. Sublimation values between 138 and 187 mm are reached. The maximum difference between hourly and daily temperature input simulations for sublimation is below 7.4% for cluster 4 (forested). The fractions of solid precipitation returned to the atmosphere ranges from 25 to 33%. Peak values are simulated for the open shaded cluster.

Table 7: Winter seasons 2021/22 sublimation values for hourly and daily temperature modelling.

Cluster	Daily Temperature					Hourly Temperature				
	Sub. canopy [mm]	Sub. ground [mm]	Sub. SUM [mm]	Total solid Prec. [mm]	Sub. Frac. [%]	Sub. canopy [mm]	Sub. ground [mm]	Sub. SUM [mm]	Total solid Prec. [mm]	Sub. Frac. [%]
A	25.7	161.1	186.7	567.6	32.90	23.8	163.1	186.9	595.4	31.39
B	111.6	36.4	147.9	462.5	31.99	105.3	36.4	141.7	476.7	29.72
C	38.9	104.4	143.3	541.1	26.48	36.6	105.2	141.8	569.3	24.91
D	118.6	29.5	148.2	455.0	32.56	110.1	27.9	138.0	441.0	31.30

3.6 Refreezing

Similar to sublimation, an evaluation of refreezing on the seasonal scale seems to be the right course of action. Refreezing values for all model runs are extracted and summarised for all model runs. Results are shown in Table 8. Refreezing ranges from 19 to 25% of the total melt. Values for hourly temperature input are generally higher than for daily temperature input. Little refreezing is taking place in the canopy layer. The majority of refrozen SWE is found in the ground layers for all clusters.

3.7 Internal Model Error

Some models do make errors in their calculations. In a hydrological model internal errors can be made visible by balancing all in- and outputs. This is done for all model runs. Therefore, the sum

Table 8: Refreezing (Ref.) values of 2021-2022 for hourly and daily temperature modelling for all four clusters.

Cluster	Daily Temperature					Hourly Temperature				
	Ref. canopy [mm]	Ref. ground [mm]	Ref. SUM [mm]	Total melt [mm]	Frac. of Ref. [%]	Ref. canopy [mm]	Ref. ground [mm]	Ref. SUM [mm]	Total melt [mm]	Frac. of Ref. [%]
A	0.1	102.1	102.2	483.0	21.15	1.0	132.4	133.4	532.4	25.07
B	0.9	77.6	78.5	393.1	19.98	3.4	102.8	106.2	441.2	24.07
C	0.1	102.5	102.6	500.5	20.50	1.5	134.3	135.8	563.3	24.11
D	0.9	71.2	72.1	379.0	19.03	3.1	85.5	88.6	391.6	22.63

of rain and snow is compared to the sublimation and outflow values of the model. No internal model error is detectable.

Table 9: Absolute model error. OUT is the sum of outflow and sublimation (canopy and ground-layer). IN is the amount of preciptation when model state is set to ON for the winter season 2021/22.

Cluster	Subl. canopy [mm]	Subl. ground [mm]	Outflow [mm]	IN [mm]	OUT [mm]	Error [mm]
Daily Temp.						
Open shaded	25.7	161.1	765.6	952.4	952.4	0
Open exposed	111.6	36.4	613.1	761.0	761.0	0
Open intermediate	38.9	104.4	756.1	899.4	899.4	0
Forested	118.6	29.5	593.2	741.4	741.4	0
Hourly Temp.						
Open shaded	23.8	164.2	780.2	968.2	968.2	0
Open exposed	105.3	36.4	624.5	766.2	766.2	0
Open intermediate	36.6	105.2	764.0	905.9	905.9	0
Forested	110.1	27.9	603.3	741.3	741.3	0

3.8 Canopy Snow Layer Evaluation

A comparison between observed an simulated snow in canopy layer is shown in Figure 9. The fraction of snow-hours correctly predicted by the model is noted in Table 10. Overall the model captures the pattern of snow days derived from the images. The model tends to simulate the quantity of snow hours better for south facing canopy snow data (compare the fraction of correctly predicted snow-hours in Table 10). Snow in the north facing canopy tends to lower melt rates than the model suggests. This effect is also observed for the south-facing canopy data, but smaller. Hourly temperature simulations show a slightly lower fraction of correctly predicted canopy snow hours.

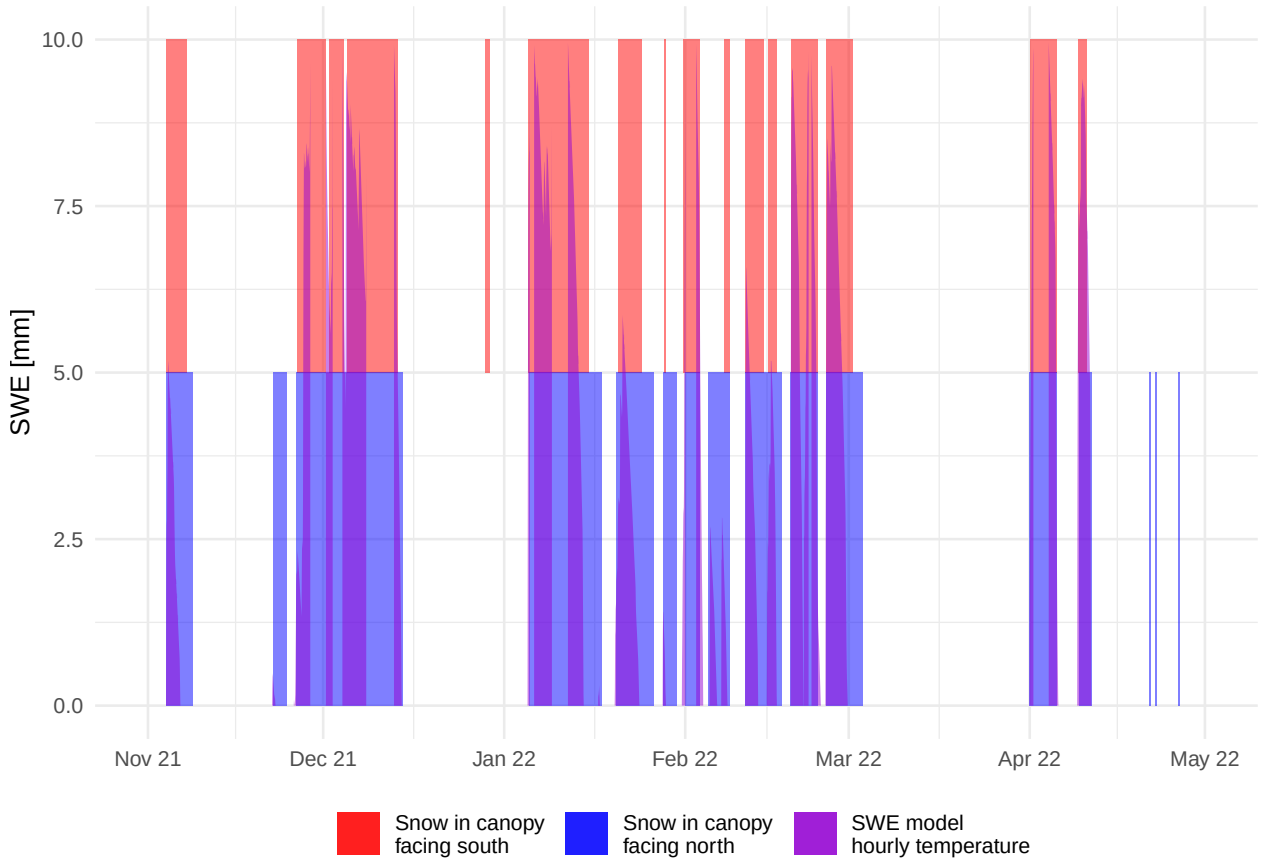

Figure 9: Comparison of model result versus visually inspected SnoMoS-data. Modelled SWE from the hourly temperature model, forested cluster are shown as the violet area exemplary. Shading in red (south-facing) and blue (north-facing) indicates the overserved snow-hours from SnoMoSs.

Table 10: The fraction of predicted snow hours that align with SnoMoS observations compared to the total predicted snow hours.

Cluster	North	South
Daily Temp.		
Open shaded	0.86	0.95
Open exposed	0.84	0.94
Open intermediate	0.85	0.95
Forested	0.82	0.93
Hourly Temp.		
Open shaded	0.85	0.95
Open exposed	0.85	0.96
Open intermediate	0.85	0.95
Forested	0.85	0.95

3.9 Rain on Snow

Figure 10 shows the model performance during rain on snow conditions. It represents a zoom in of the previously mentioned model run (hourly temperature, model for forested cluster). Shown are

a temperature and precipitation digram, a SWE-Plot with simulation results from this work and the results from Geissler, Rathmann, and Weiler (2023) as comparison. Outflow and snow-layer saturation were plotted to supplement additional internal model data for evaluation. In their work Geissler et al. described one ROS event in late December. It was recorded after three days of mild rain. Starting on 2021-12-27 the precipitation increased and melt rates amplified accordingly. Rain was falling until the 29th of December. From then on temperatures increased again and the warm period continued until 2022-01-04 (A). Overall the model is able to simulate the ROS events in a general manner. Melt rates during the main rain melt phase from 27th to 30th are predicted too low. Melt rates during the following warm phase seem to be quite accurate. After noon on the 24th liquid content in the snow-cover is not rising any more (B). This also can be seen in the outflow graph (C). Outflow starts at noon the 24th following the precipitation pattern. Maximum values are reached on the 29th. In the following period with no precipitation outflow resembles the temperature graph.

Numerical data for the event were supplied (Table 11) to gain insight into the leading processes driving the melting of the snow-pack. Precipitation was about 84 mm for the whole period. Some is reaching the ground directly, the other part through dripping from canopy. The amounts of dripping are mostly equal between hourly and daily temperature models. A small fraction of solid snow is unloaded from canopy, presumed from the snow event on the 29th. Rain-melt is in between 4.2 and 4.7 mm and similar for all clusters and inputs. Rain melt rates play a relatively small role in ROS melt when compared to temperature melt. Temperature melt is approximately 5 to 7 times higher than rain-melt. Highest temperature melt is modelled for the forested cluster.

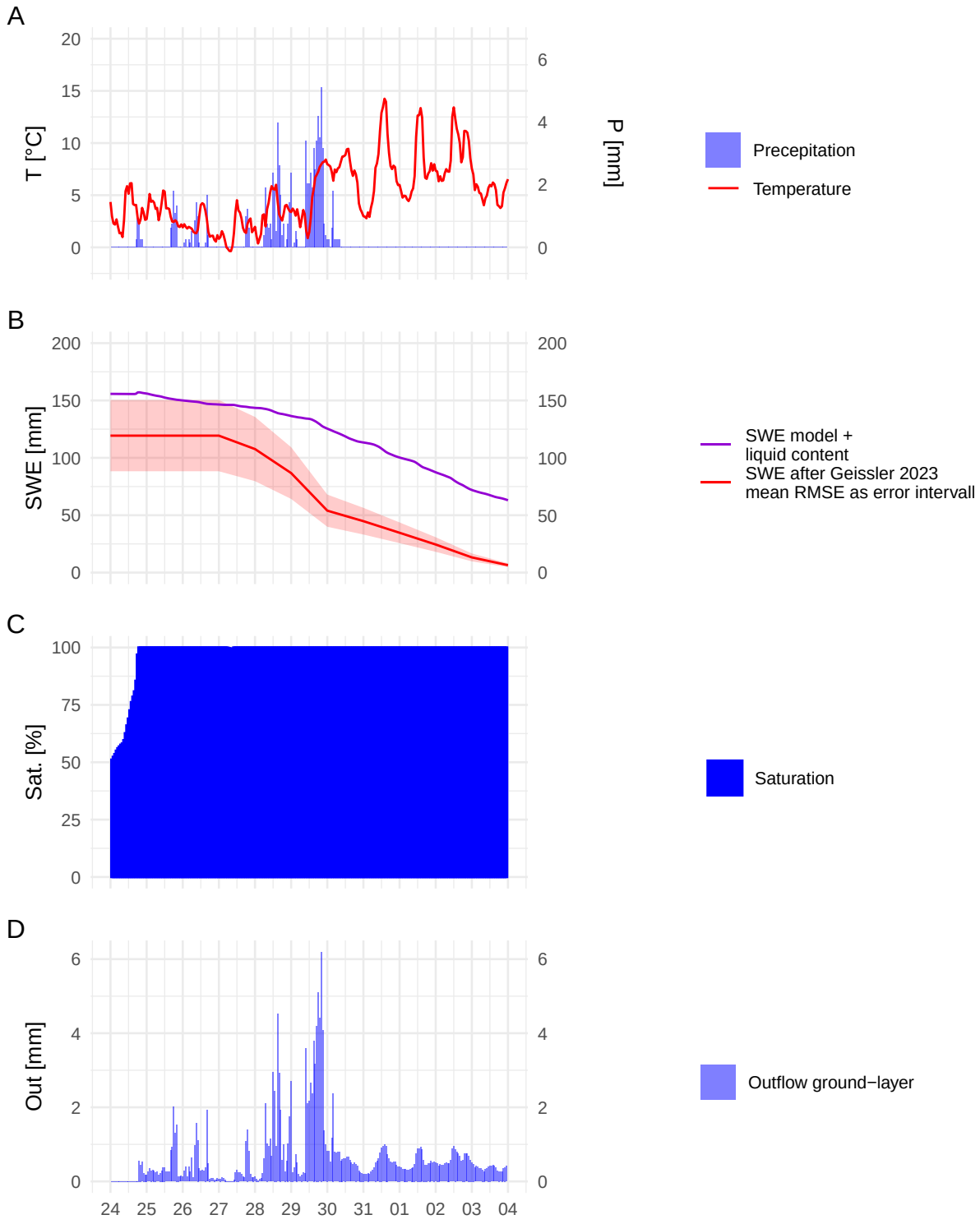

Figure 10: Climate and model data for the ROS event between 2021-12-27 5:00 PM and 2022-01-04 0:00 AM. Precepitation is shown as Richter corrected values provided by the model (A). Modelled SWE for the forested cluster with hourly temperature input is plotted in (B). The Geissler 2023 timeseries with mean RMSE as error intervall is shown as reference. Saturation (C) and outflow (D) are directly obtained from the model output.

Table 11: Cumulative values for richter-corrected precepitation (P), throughfalling precipiation (P ground), dripping from canopy layer (D), melt values (M) for rain and temperature melt the ground outflow (O). The event time was set in between 2021-12-24 12:00 AM and 2021-12-30 06:00 PM.

Cluster	P total [mm]	P liquid ground [mm]	D [mm]	M rain [mm]	M temp. [mm]	O [mm]
Daily Temp.						
Open shaded	83.7	66.9	16.7	4.2	22.8	110.0
Open exposed	83.7	50.2	33.5	4.2	25.2	112.1
Open intermediate	83.7	58.6	25.1	4.2	24.9	111.8
Forested	83.7	16.7	66.9	4.2	28.6	114.7
Hourly Temp.						
Open shaded	83.6	66.9	16.7	4.7	23.2	110.1
Open exposed	83.7	50.2	33.5	4.7	25.9	113.0
Open intermediate	83.6	58.5	25.1	4.7	25.5	112.5
Forested	83.7	16.7	66.9	4.7	29.2	116.3

4 Discussion

4.1 Model Structure

In the context of this master thesis, it's important to acknowledge that while the snow model's structure has been meticulously designed, based on current knowledge of snow physics and meteorology, its actual performance within the Roger program remains uncertain. As the author of this thesis, I am not directly involved in the implementation process, making it challenging for me to definitively assess how well the model's structure will integrate with RoGeR's existing framework and contribute to its predictive capabilities. The effectiveness of the model within the RoGeR program can only be determined through the practical implementation and subsequent evaluation by experts responsible for its integration. This thesis lays the theoretical groundwork, but the model's real-world performance and compatibility will ultimately unfold during its implementation phase.

4.2 Internal Model Error

As a first step in model evaluation, the internal model error was examined. As shown the model does not exhibit any internal errors. This is proof for the basic functionality of the program. For future research, it is essential to acknowledge that, owing to the Richter precipitation correction, a greater amount of precipitation exits the model than initially provided. Following the Richter

correction, all incoming water is accounted for through a combination of sublimation and outflow processes. For a quantification of the increase in precipitation for both modelled seasons see Table 12 in the appendix.

4.3 Model Parameters

The evaluation of model parameters plays a crucial role in assessing a physics based model. The values assigned to these parameters provide valuable insights into the model's representation of underlying processes. Estimating the credibility of model parameters that describe snow mechanisms offers a possibility to understand how effectively the model predicts these processes' dynamics.

4.3.1 Liquid Storage Coefficient

Of these parameters, the storage coefficient holds particular significance as it dictates the snow cover's capacity to retain water. This, in turn, plays a role in initiating melt processes. Prior to reaching saturation, the snow cover stores water. That has the potential to freeze during night-time. The determination of the storage coefficient is informed by existing literature (Koch et al. 2014; Mitterer et al. 2011; Saelthun 1996). All liquid water contained within the snow cover contributes to the SWE.

The model aptly captured the onset of melt events during the 2021/22 calibration season. Slight ablation in between the melt events could be tracked down to sublimation losses. Notably, there exists no discernible bias in melt timing (compare Figure 8), implying the overall appropriateness of the chosen storage coefficient. However, in the previous season (2020/21), the model predicted a mid-winter melt event for all clusters in late January. The melt event is not present in the reference ΔSnow data. This could be caused by inaccuracies of the ΔSnow model. Potentially, modelling with a higher storage capacity could have led to a higher fraction of water stored in the snow cover for later refreezing. This could have lessened the effects of the melt and therefore enhanced model precision. On the other hand spring melt in April was predicted late. Potentially the state of the snow pack did not allow for any more liquid water to be stored. This could be due to previous refreezing processes, densifiying the snow cover and lowering the water holding capacity. In this context, the pursuit of more intricate solutions, such as coupling water holding capacity with a snow state simulation - largely dictated by snow temperature and density - might

be imperative. The challenges associated with acquiring liquid content measurements at a high spatial resolution are highlighted by previous work (Techel and Pielmeier 2011). In the absence of well-verified data suitable for rigorously testing complex methodologies, the utilization of the storage coefficient approach remains pragmatic and judicious.

4.3.2 Refreezing Rate

Liquid water within the snow cover has the potential to undergo refreezing. The Nordic HBV model treats refreezing like melt processes, employing a DDF. However, in this configuration, the DDF was intertwined with a refreezing efficiency factor set at 5%. This implies that the refreezing process operates at a rate 20 times slower than melting. The rationale behind this specific efficiency factor remains elusive, as no relevant literature elucidates its basis. Consequently, for the scope of this study, a pragmatic assumption is made: Refreezing is assumed to occur at the same rate as melting. Therefore, the refreezing rate is calibrated to 1. In the absence of validation data for refreezing in sub-alpine catchments, the annual amount of refreezing which is roughly 50% of annual glacial refreezing seems plausible. It is worth noting that, should future investigations yield evidence to the contrary, adjusting the refreezing mechanism within this model is straightforward. This adaptable nature of the refreezing parameter allows for flexibility and refinement in light of more comprehensive insights gained from subsequent studies. A more thorough discussion on this topic could be found in chapter 3.6 Refreezing.

4.3.3 Unloading Factor

The subsequent parameter to discuss is the unloading factor. Much of the algorithm pertaining to this factor is rooted in research conducted by Hedstrom and Pomeroy (1998). Formulas for both the maximum load and interception efficiency were obtained through this research. The formula for unloading was slightly altered. Hedstrom delineates an exponential decay with the unloading rate coefficient as the exponent's base, set to the value of 'e'. In the modified version, the approach remains exponential decay, but the unloading rate coefficient is integrated into the base of the formula. Consequently, a fixed percentage defined by the unloading factor of the initial snow load in the canopy is shed every day. This approach appears more intuitive and should still yield similar outcomes. With respect to Table 10, this method seems to perform well. Approximately 95% of the southern snow accumulation time in the canopy was accurately predicted. Further insights are

provided in Figure 9. Decreases in canopy SWE occur much more rapidly than the 10% per day rate implied by unloading. As a result, it's plausible to assume that in this model, most of the reduction in canopy SWE occurred due to melting and sublimation rather than unloading. This complexity makes evaluating unloading challenging. However, despite this intricacy, the model's outcomes consistently match the observed data, whether due to factors that are comprehensible or those that remain unknown. Due to the difference in model performance for south and north facing canopy a split routine for south and north facing canopy could improve model results in the future.

4.3.4 Canopy Coverage and LAI

Shifting focus to the factors affecting snow processes in canopy, both canopy coverage and LAI play pivotal roles in influencing refreezing and sublimation processes. The values utilized for the simulations in this study are mean cluster values extracted automatically from Geissler, Rathmann, and Weiler (2023). It's worth noting that, for instance, the open and exposed cluster does not truly exhibit a canopy coverage of 0.4. This value arises due to branch overlap at the cluster's edge areas or the presence of small bushes in open spaces. This kind of vegetation plays a role distinct from that of a fully developed forest. Such vegetation is rapidly covered by snow and subsequently ceases to significantly impact snow processes. Nevertheless, the decision was made to incorporate these parameters values into the model. The rationale behind this decision is that if these clusters are to be derived from future work using satellite imagery or LiDAR data, these artefacts will persist. Consequently, it was sensible to integrate these parameters into the simulation.

4.3.5 Degree-Day-Factor Calibration

A variety of DDF values have been documented in literature, with their specifics influenced by the location of the model application. An essential differentiation can be made between DDF values for snow and ice. Notably, the DDF employed in this model was designed exclusively for simulating snow-melt. Drawing from the methodology presented in Hock (1999), the model integrates a base DDF with a radiation DDF.

The model's radiation-based DDF extends the base DDF to 2.5 $°C^{-1}day^{-1}$ at noons in April. No DDF is calculated when the model state is in "off" position. For more detailed information see

Figure 12 in the appendix. Conventionally, DDF values exhibit an upward trend with increasing altitude, varying due to seasonal changes, cloud cover, and specific events such as ROS, as noted in (Ismail et al. 2023).

Considering the amalgamation of these factors and conducting comparisons with other snow models like (Saelthun 1996; Valery 2010; "SNTHERM" 2012), the DDF range adopted in this study appears plausible. In reference to Figure 8, the observed melt rates demonstrate a fitting correspondence (with the exception of the ROS event).

It's worth considering that the sublimation, which was unaccounted for in the ΔSnow modelled SWE data, could potentially explain the discrepancy of slightly under 200 mm at the 2020/21 season's end between the results of Geissler, Rathmann, and Weiler (2023) and the simulation data (Figure 8). Therefore this is not due to underestimated melt rates. Underestimated melt rates in April 2022 were reported to be caused by a shara-dust event, decreasing albedo and therefore increasing melt (Geissler, Rathmann, and Weiler 2023). This is not captured by the model.

4.3.6 Snowfall Temperature

The average snowfall temperature across the northern hemisphere was reported to be 1.0 °C, with 95% of all stations (n = 17.8 million) falling within the range of -0.4 to 2.4 °C, as documented by (Jennings et al. 2018). Notably, the snowfall temperatures used for modelling all four clusters are well within this range. The proposition of lower snowfall temperatures in forested regions, influenced by heightened long wave radiation within forests, appears reasonable. It's important to acknowledge that snowfall temperature isn't static; rather, it's dependent on relative humidity among other factors. Models that consider this interrelation tend to yield better results compared to those that do not, as noted by Jennings et al. (2018).

Turning attention to Figure 7, the fixed-threshold temperature approach demonstrates a commendable performance. This is especially evident when accounting for the aforementioned sublimation effects.

Nevertheless, some snow events are not accurately captured. This is exemplified by the early February event of the 2021/22 period. The model predicted snowfall, which isn't corroborated by the Geissler, Rathmann, and Weiler (2023) data. The same is true for the late January event in the 2020/21 season. The magnitude of most other snowfall events was captured well in both seasons.

These disparities indicate that snowfall temperature is not constant trough the season. Enhancing the snow module with a bulb-temperature approach could yield improved outcomes, provided humidity data is accessible. Considering the model's high sensitivity to the threshold temperature this could be a starting point for model enhancement. For more information on model sensitivity look at Figure 13 in the appendix. This prospective extension could potentially be a focus for future research endeavours, aimed at refining the model's predictive capabilities.

4.3.7 Shade

The determination of the shading parameter is contingent upon the spatial placement of the clusters. This shading component finds its incorporation within the radiation portion of the DDF. While the base DDF remained consistent across all clusters, divergence emerges concerning the radiation DDF. For the open-intermediate cluster, a 90% reduction was applied to the radiation DDF (with a 50% reduction for the open shaded cluster).

However, these modifications may potentially result in slightly lower melt rates during the spring of 2021 (as depicted in Figure 6). This observation triggers a consideration: The shading effect might have been somewhat overestimated. While the shading values themselves appear to be reasonably set, it's conceivable that a recalibration could be beneficial.

To address this potential issue, future model iterations could contemplate a dual approach: Diminishing the influence of the radiation DDF while concurrently elevating the base DDF. This calibrated adjustment might offer a resolution to the challenges currently encountered in the model.

4.4 Comparison of Annual Sublimation Values

Not specifically parametrized in this model sublimation is a direct consequence of potential evaporation. Available energy derived from potential evaporation is calculated and refereed to the sublimation of snow. This way the amount of potential sublimation is calculated. The referred values ranging from 125 to 187 mm (refer to Table 7) align with findings from comparable literature concerning a location at an elevation of 1200 m.a.s.l. (Strasser et al. 2008). Strasser's outcomes indicate that the majority of sublimation originates from the canopy when present, a conclusion corroborated by the model presented in this study. This observation holds true for both forested and non-forested regions in terms of the amount of sublimation. Further testing in diverse climates

and altitudes is imperative to validate these outcomes. Accordingly the altitude effect could be implemented in later versions of the snow module if this proves necessary.

4.5 Hourly and Daily Temperature Input Modelling

A marginal enhancement in model outcomes was observed when employing hourly temperature data for modelling purposes. In instances where hourly temperature data is inaccessible, modelling based on daily temperature data remains a viable approach (compare Figure 5 and 6).

However, this proposition does not hold true for the forested clusters. A noticeable difference in KGE values is evident during validation and calibration period between the two temperature input methods (compare Table 6). This discrepancy in temperature inputs is also reflected in the reduced RMSE and MAE values for models utilizing hourly temperature data.

The question for the dominant processes responsible for the anomalous behaviour within this cluster arises. Comparatively similar seasonal sublimation values are obtained when considering hourly versus daily temperature inputs (see Table 7). Hence, it is reasonable to assume that sublimation is not the primary driver behind this observed variance. Notably, disparities in refreezing values emerge between models employing hourly and daily temperature inputs across all clusters. Hourly temperature models exhibit an increment in the proportion of refrozen water (see Table 8). This suggests that the phenomenon of refreezing could play a pivotal role when modelling forested regions.

Moreover, the temporal distribution of precipitation emerges as another influential factor. Particularly in clusters characterized by higher snowfall temperatures, such as open intermediate and open shaded clusters, this variance is more pronounced. This phenomenon is visibly exemplified in events like early February 2021, where a discrepancy between the SWE modelled using hourly and daily temperature inputs is discernible in the forested cluster. This trend extends to subsequent periods of snow fall throughout the remainder of February.

Lastly the inclusion of hourly temperature modelling brings about effects that might not be immediately apparent when solely focusing on the primary model output, which in this case is SWE. However, when considering the patterns in outflow, the significance of this hourly modelling becomes evident. As shown in Figure 10, discernible patterns emerge in the outflow behaviour.

Notably, periods of warm weather exhibit heightened outflow during daytime and diminished outflow during night time when temperatures drop. This is particularly pertinent when the point of saturation has already been attained. When simulating with daily temperature input this dynamic is less intense. If the model time step is chosen small enough, higher melt rates during day time due to radiation effects can be simulated (see Figure 12 in the appendix). Moreover, the occurrence of refreezing during night time can introduce a slowdown in the process of reaching saturation. As previously mentioned, the hourly model runs tend to yield increased refreezing rates. These dynamics potentially hold implications for the behavior of released water on soil surfaces. Higher outflow during daytime periods might contribute to heightened surface runoff and reduced rates of infiltration. To comprehensively assess the magnitude of these effects, it is imperative to conduct further testing following the implementation of this module in the RoGeR model. Through such investigations, a clearer understanding of the hydrological consequences stemming from hourly temperature modelling can be gleaned.

In conclusion, the utilization of hourly temperature data leads to marginal improvements in SWE modelling outcomes. While the open shaded, open intermediate and open exposed clusters can be effectively modelled using daily temperature data, this approach is insufficient for accurately capturing dynamics within the forested clusters. The dissimilarities in refreezing fractions and the temporal distribution of precipitation underscore the importance of these factors in explaining the observed discrepancies. Further investigation is warranted to comprehensively elucidate the underlying processes driving these distinctions in model behaviour. The inclusion of hourly temperature modelling yields subtle yet significant effects on outflow patterns. This bears implications for surface runoff and infiltration, requiring further evaluation following the implementation of this module in the RoGeR model.

4.6 Challenges in Rain on Snow Simulation

Rainfall on snow is a frequent contributor to flooding, as noted by Beniston and Stoffel (2016). Consequently, it holds significance when integrating snow with soil models. Examining the modelled ROS event in December 2021 warrants further discussion. The utilization of daily or hourly temperature data does not yield distinguishable differences in the overall discharge, nor does it impact temporal discharge patterns. Under ROS and saturated snow cover conditions, the model projects a runoff pattern that aligns with the precipitation sequence.

The input precipitation interval for RoGeR was set at 10 minutes. Additionally a high-resolution temperature dataset is imperative when simulating runoff patterns during melting conditions. This becomes evident in the period subsequent to the ROS event, particularly when melting is driven by temperature (Figure 10). Neither the daily nor the hourly temperature models accurately capture the melt rates during the ROS event (Figure 5). While the temperature-induced melting rates match post-ROS period, they underestimate the melting that transpires during the ROS event itself.

The model distinctly calculates the energy released from warm rain interacting with the snow cover. The computed rain-induced melt amounts to roughly one-fifth of the temperature-induced melt for the entire ROS event duration (Table 11). This appears to be adequate for modelling clusters adjacent to forested regions, such as the open intermediate and open shaded clusters. However, it falls short when applied to modelling open exposed and forested clusters, where melt rates tend to be higher.

ROS leads to elevated melt rates in both forested and open areas, surpassing rates in areas proximate to forests. A comparative study of melt events and associated energy flux measurements on and from the snow cover yields the following outcomes: In open environments, turbulent heat exchanges do have a major impact on the distribution of surface energy. During two observed periods of ROS events within forests, the primary factors influencing this energy balance are the turbulent exchange of sensible and latent heat, as well as the net longwave radiation (Garvelmann 2014). In clusters located near forests, wind speed tends to be lower. Moreover, the quantity of energy penetrating the snow pack from longwave radiation is diminished compared to forested areas. It is possible that spatial patterns in precipitation distribution result in decreased input of rain energy in regions close to forests. Further research should focus on elucidating the reasons behind the variations in melt rates among the clusters under ROS conditions.

4.7 Evaluation of the Cluster Modelling Approach

When evaluating the results of this study, two key points hold significance. Firstly, only one year of calibration data is available, and similarly, only one year of validation data is accessible. While no studies have specifically addressed model performance concerning the calibration period for snow models, there have been studies that compare performance with varying calibration periods for hydrological models.

One of these studies evaluated the GR4J model coupled with the snow module CemaNeige. The evaluation demonstrated a slight improvement in model performance with each new year of calibration data. However, noteworthy model efficiencies were already observed in the first year, indicated by the Nash-Sutcliffe Efficiency (NSE) values, which fell within 90% of the maximum achieved NSE (Ayzel and Heistermann 2021). This suggests that the GR4J conceptual model and the CemaNeige snow model perform well even with short calibration data periods.

The model developed within the scope of this work is also a conceptual, physically-based model. This model also does exhibit good performance with a concise calibration time series. A calibration period of one year proves to be sufficient to yield accurate modelling results for the subsequent year. This contrasts with the findings of Essery et al. (2009), where a one-year calibration period does not guarantee satisfactory model outcomes.

Overall, modelling with hourly temperature input ensures good KGE values for all clusters during the validation season. KGE values during the calibration seasons are even higher. The challenge of diminished model performance associated with daily temperature input appears to be partly resolvable through specific calibration for daily temperature input. Further model testing is required to validate this approach.

The modelled time series for both seasons indicate that particularly in the forested clusters, processes are simulated differently based on temperature input resolution. Consequently, future research efforts should concentrate on quantifying these disparities through extensive model testing using additional test data. Emphasis should be placed on analyzing refreezing, day-night melt cycles, and accumulation patterns, particularly for the forested cluster. This concerted focus will contribute to a more comprehensive understanding of the model's behaviour and capabilities.

4.8 Future Research: Enhancing Snow Model Performance

In the realm of advancing the capabilities of the snow model, there exist several prospects for further investigation. This delves into these potential avenues of research, refining the existing snow model and augment its applicability.

1. Extended model testing with clustered snow data: In the pursuit of improving the current snow model's capabilities, future research could delve deeper into extensive model testing using clustered snow data. This data should match the clustering structure from this studys test site. By exploring various seasons and examining how the model performs with each distinct set of conditions, a more comprehensive understanding of its adaptability and robustness can be gained.

2. Identifying new clusters and model testing: Expanding the scope, researchers could identify additional clusters that may have been previously overlooked. Testing the existing model against these newly identified clusters can provide insights into its versatility and potential limitations under diverse conditions.

3. Extracting cluster data from LiDAR or satellite sources: In a bid to enhance data collection techniques, a path of exploration involves deriving cluster-specific data from LiDAR or satellite sources.

4. Integrating with RoGeR and structural adaptations: The future evolution of the snow model encompasses its integration into RoGeR. As such, investigating potential structural changes required for seamless incorporation could unveil new opportunities for synergistic modelling approaches.

5. Application and validation in diverse catchments: To ascertain the model's adaptability beyond its current scope, applying and validating together with RoGeR in various catchments with abundant validation data holds paramount importance. This step ensures that the model's efficacy is tested across a range of environmental and climatic conditions.

6. Upscaling to larger geographic areas: Expanding the model's domain to encompass larger geographical areas offers an exciting challenge. Scaling up requires addressing intricate spatial and temporal dynamics while maintaining accuracy. This endeavour could open doors to forecasting snow-related phenomena over expansive regions.

5 Conclusion

The snow module was initially developed for subsequent integration into the RoGeR framework. A requirement exists for additional assessments to ascertain the compatibility of the model structure with RoGeR. Clustered SWE data were acquired and assessed for model testing. This was done to create a model with reduced complexity, input parameter count, and boosted simulation efficiency.

The model's input requirements were streamlined to the most essential components. This encompasses a time series of temperature and precipitation with varying resolution, and a time series of daily evapotranspiration. Consequently, a straightforward model structure was formulated, employing a dual-DDF approach alongside a threshold-based separation for temperature and precipitation. Furthermore, the model incorporates routines for liquid water, refreezing processes, sublimation and ROS-events. The input parameters have been reasonably set to represent the underlying physical processes.

The model has successfully demonstrated its capacity to adequately simulate canopy SWE, based on this set of input data. Accumulation and ablation rates are predicted well when accounting for the lack of sublimation in the reference data. Sublimation is evaluated on an annual scale matching the corresponding values described in literature. Annual refreezing values seem plausible. No internal errors could be detected in the model's architecture. Overall, the model has exhibited commendable performance with only short periods of calibration data.

The quality of the model's outputs is contingent upon the resolution of input temperature data. A slight improvement of model results is visible when using hourly temperature as input. The improvement in simulation results varies in between the clusters. For the forested areas the increase in model performance is higher than for the other clusters. This divergence is could be attributed to dissimilarities in processes like diurnal melt cycles, refreezing, and precise distinction between solid and liquid precipitation. DDF values during day time are higher for hourly temperature input. The same could be shown for refreezing during night time. As a result hourly temperature data becomes important when capturing detailed outflow patterns. Precipitation is separated differently when temperature input resolution changes. This is especially true for the open-exposed and the forested cluster. Those clusters exhibit the lowest threshold temperature for snowfall. Resulting

errors accumulate over the season. Enhanced model performance may be attainable by calibrating specifically for daily temperature data.

A notable factor contributing to diminished model performance pertains to inadequate modelling of ROS events. ROS occurrences induce distinct melt rates among clusters. Clusters situated near forested regions displayed lower melt rates compared to both forested and open exposed clusters. The model notably underestimates melt rates in the forested and open exposed clusters. Pinpointing the precise cause necessitates future investigations. Potential starting points include the examination of precipitation distribution, variations in wind speed, and the equilibrium of longwave radiation.

Future research endeavours concerning this model should adhere to the following trajectory: Expanded model testing with clustered snow data, identification and testing of new clusters, cluster data extraction from LiDAR or satellite sources, integration with RoGeR and accompanying structural adaptations, application and validation in diverse watersheds, and scaling to larger geographic regions. Eventually, these efforts aim to yield simplified, efficient, and robust snow models with global applicability.

6 References

AeroPythonTeam. 2019. "Solyrpy: Python Solar Radiation Model."

Ayzel, Georgy, and Maik Heistermann. 2021. "The Effect of Calibration Data Length on the Performance of a Conceptual Hydrological Model Versus LSTM and GRU: A Case Study for Six Basins from the CAMELS Dataset." *Comput. Geosci.* 149 (April): 104708.

Becherini, Francesca, Vito Vitale, Angelo Lupi, Robert S Stone, Rosamaria Salvatori, Roberto Salzano, Piero di Carlo, Angelo Pietro Viola, and Mauro Mazzola. 2021. "Surface Albedo and Spring Snow Melt Variations at Ny-Ålesund, Svalbard." *Bulletin of Atmospheric Science and Technology* 2 (1): 14.

Behrangi, Ali, Xungang Yin, Seshadri Rajagopal, Dimitrios Stampoulis, and Hengchun Ye. 2018. "On Distinguishing Snowfall from Rainfall Using Near-surface Atmospheric Information:comparative Analysis, Uncertainties and Hydrologic Importance." *Quart. J. Roy. Meteor. Soc.* 144 (S1): 89–102.

Beniston, Martin, and Markus Stoffel. 2016. "Rain-on-Snow Events, Floods and Climate Change in the Alps: Events May Increase with Warming up to 4°c and Decrease Thereafter." *Sci. Total Environ.* 571 (November): 228–36.

Conway, H, A Gades, and C F Raymond. 1996. "Albedo of Dirty Snow During Conditions of Melt." *Water Resources Research* 32 (6): 1713–18.

Cox, C, N Humphrey, and J Harper. 2015. "Quantifying Meltwater Refreezing Along a Transect of Sites on the Greenland Ice Sheet." *Cryosphere* 9 (2): 691–701.

Davidov, S, D Marks, G Flerchinger, and D Garen. 2004. "Linking an Energy-Balance Snow Model (SNOBAL) to a Soil Temperature and Moisture Model (SHAW)." In, 2004:C31A–0286.

Duffie, John A. 1974. *Solar Energy Thermal Processes.* Wiley.

Essery, Richard. 2015. "A Factorial Snowpack Model (FSM 1.0)." *Geoscientific Model Development* 8 (12).

Essery, Richard, Nick Rutter, John Pomeroy, Robert Baxter, Manfred Stähli, David Gustafsson, Alan Barr, Paul Bartlett, and Kelly Elder. 2009. "Snowmip2: An Evaluation of Forest Snow Process Simulations." *Bull. Am. Meteorol. Soc.* 90 (8): 1120–36.

Etchevers, P, E Martin, R Brown, C Fierz, Y Lejeune, E Bazile, A Boone, et al. 2004. "Validation of the Surface Energy Budget Simulated by Several Snow Models (SnowMIP Project)." *Ann. Glaciol.* 38: 150–58.

Förster, Kristian, Jakob Garvelmann, Gertraud Meißl, and Ulrich Strasser. 2018. "Modelling

Forest Snow Processes with a New Version of WaSiM." *Hydrol. Sci. J.* 63 (10): 1540–57.

Garvelmann, Jacob. 2014. "Observations of the Spatial and Temporal Variability of Snowmelt Energetics and Runoff Generation During Rain-on-Snow in a Forested Mid-Latitude Mountain Environment." Edited by Markus Weiler. PhD thesis, Albert-Ludwigs-University.

Geissler, Joschka, Lars Rathmann, and Markus Weiler. 2023. "Combining Daily Sensor Observations and Spatial LiDAR Data for Mapping Snow Water Equivalent in a Sub-alpine Forest." *Water Resour. Res.*, August.

Grolemund, Garrett, and Hadley Wickham. 2011. "Dates and Times Made Easy with lubridate." *Journal of Statistical Software*.

Guo, Danlu, Seth Westra, and Holger R Maier. 2016. "An R Package for Modelling Actual, Potential and Reference Evapotranspiration." *Environmental Modelling & Software* 78 (April): 216–24.

Gupta, Hoshin V, Harald Kling, Koray K Yilmaz, and Guillermo F Martinez. 2009. "Decomposition of the Mean Squared Error and NSE Performance Criteria: Implications for Improving Hydrological Modelling." *J. Hydrol.* 377 (1): 80–91.

Harris, Charles R, K Jarrod Millman, Stéfan J van der Walt, Ralf Gommers, Pauli Virtanen, David Cournapeau, Eric Wieser, et al. 2020. "Array Programming with NumPy." *Nature* 585: 357–62.

Hedstrom, N R, and J W Pomeroy. 1998. "Measurements and Modelling of Snow Interception in the Boreal Forest." *Hydrol. Process.* 12 (10-11): 1611–25.

Henderson-Sellers, A, A J Pitman, P K Love, P Irannejad, and T H Chen. 1995. "The Project for Intercomparison of Land Surface Parameterization Schemes (PILPS): Phases 2 and 3." *Bull. Am. Meteorol. Soc.* 76 (4): 489–503.

Henderson-Sellers, B. 1984. "A New Formula for Latent Heat of Vaporization of Water as a Function of Temperature." *Quart. J. Roy. Meteor. Soc.* 110 (466): 1186–90.

Hijmans, Robert J. 2023. "Raster: Geographic Data Analysis and Modeling."

Hock, Regine. 1999. "A Distributed Temperature-Index Ice- and Snowmelt Model Including Potential Direct Solar Radiation." *J. Glaciol.* 45 (149): 101–11.

Iglesias, Ana, Dionysis Assimacopoulos, and Henny A J Van Lanen, eds. 2018. *Drought: Science and Policy*. Hydrometeorological Extreme Events. Standards Information Network.

Ismail, Muhammad Fraz, Wolfgang Bogacki, Markus Disse, Michael Schäfer, and Lothar Kirschbauer. 2023. "Estimating Degree-Day Factors of Snow Based on Energy Flux Components." *Cryosphere* 17 (1): 211–31.

Jennings, Keith S, Taylor S Winchell, Ben Livneh, and Noah P Molotch. 2018. "Spatial Variation of the Rain-Snow Temperature Threshold Across the Northern Hemisphere." *Nat. Commun.* 9 (1): 1148.

Jordan, Rachel E, Edgar L Andreas, and Aleksandr P Makshtas. 1999. "Heat Budget of Snow-Covered Sea Ice at North Pole 4." *J. Geophys. Res.* 104 (C4): 7785–7806.

Jorgenson, T M, Vladimir Romanovsky, Jennifer Harden, Yuri Shur, and Sergei Marchenko. 2010. "Resilience and Vulnerability of Permafrost to Climate Change." *Can. J. For. Res.* 40 (7): 1219–36.

Koch, Franziska, Monika Prasch, Lino Schmid, Jürg Schweizer, and Wolfram Mauser. 2014. "Measuring Snow Liquid Water Content with Low-Cost GPS Receivers." *Sensors* 14 (11): 20975–99.

Krinner, Gerhard, Chris Derksen, Richard Essery, Mark Flanner, Stefan Hagemann, Martyn Clark, Alex Hall, et al. 2018. "ESM-SnowMIP: Assessing Snow Models and Quantifying Snow-Related Climate Feedbacks." *Geosci. Model Dev.* 11 (12): 5027–49.

Lehning, Michael, Perry Bartelt, Bob Brown, Tom Russi, and Martin Zimmerli. 1999. "SNOWPACK Model Calculations for Avalanche Warning Based Upon a Network of Weather and Snow Stations." *Cold Reg. Sci. Technol.* 30 (1-3): 145–57.

Li, Dongyue, Dennis P Lettenmaier, Steven A Margulis, and Konstantinos Andreadis. 2019. "The Role of Rain-on-snow in Flooding over the Conterminous United States." *Water Resour. Res.* 55 (11): 8492–8513.

Lumbrazo, Cassie, Andrew Bennett, William Ryan Currier, Bart Nijssen, and Jessica Lundquist. 2022. "Evaluating Multiple Canopy-snow Unloading Parameterizations in SUMMA with Time-lapse Photography Characterized by Citizen Scientists." *Water Resour. Res.* 58 (6).

Mahat, Vinod, and David G Tarboton. 2014. "Representation of Canopy Snow Interception, Unloading and Melt in a Parsimonious Snowmelt Model." *Hydrol. Process.* 28 (26): 6320–36.

Mazzotti, Giulia, Richard Essery, C David Moeser, and Tobias Jonas. 2020. "Resolving Small-Scale Forest Snow Patterns Using an Energy Balance Snow Model with a One-Layer Canopy." *Water Resour. Res.* 56 (1): e2019WR026129.

Mazzotti, Giulia, Richard Essery, Clare Webster, Johanna Malle, and Tobias Jonas. 2020. "Process-level Evaluation of a Hyper-resolution Forest Snow Model Using Distributed Multisensor Observations." *Water Resour. Res.* 56 (9).

Mazzotti, Giulia, Clare Webster, Richard Essery, and Tobias Jonas. 2021. "Increasing the Physical Representation of Forest-snow Processes in Coarse-resolution Models: Lessons Learned from

Upscaling Hyper-resolution Simulations." *Water Resour. Res.* 57 (5).

McKinney, Wes, and Others. 2010. "Data Structures for Statistical Computing in Python." In *Proceedings of the 9th Python in Science Conference*, 445:51–56. Austin, TX.

Mitterer, Christoph, Achim Heilig, Schweizer, Jürg, and Olaf Eisen. 2011. "Upward-Looking Ground-Penetrating Radar for Measuring Wet-Snow Properties." *Cold Reg. Sci. Technol.* 69 (2): 129–38.

Natali, Susan M, Jennifer D Watts, Brendan M Rogers, Stefano Potter, Sarah M Ludwig, Anne-Katrin Selbmann, Patrick F Sullivan, et al. 2019. "Large Loss of Co2 in Winter Observed Across the Northern Permafrost Region." *Nat. Clim. Chang.* 9 (November): 852–57.

Pedersen, Thomas Lin. 2020. "Patchwork: The Composer of Plots."

Penman, Howard Latimer, and Bernard Augustus Keen. 1948. "Natural Evaporation from Open Water, Bare Soil and Grass." *Proc. R. Soc. Lond. A Math. Phys. Sci.* 193 (1032): 120–45.

Pomeroy, John W, and R A Schmidt. 1993. "The Use of Fractal Geometry in Modelling Intercepted Snow Accumulation and Sublimation." In *Proceedings of the Eastern Snow Conference*, 50:1–10. westernsnowconference.org.

Pomeroy, J, J Parviainen, N Hedstrom, and D Gray. 1998. "Coupled Modelling of Forest Snow Interception and Sublimation." *Hydrol. Process.*

Python Software Foundation. 2021. "datetime - Basic Date and Time Types." https://docs.python.org/3/library/datetime.html.

Richter, Dieter. 1995. "Ergebnisse Methodischer Untersuchungen Zur Korrektur Des Systematischen Meßfehlers Des Hellmann-Niederschlagmessers." *Berichte Des Deutschen Wetterdienstes* 194.

Saelthun, Niels Roar. 1996. "THE 'NORDIC' HBV MODEL." *NORWEGIAN WATER RESOURCES AND ENERGY ADMINISTRATION*, July.

Schmidt, R A, and David R Gluns. 1991. "Snowfall Interception on Branches of Three Conifer Species." *Can. J. For. Res.* 21 (8): 1262–69.

Slater, A G, C A Schlosser, C E Desborough, A J Pitman, A Henderson-Sellers, A Robock, K Ya Vinnikov, et al. 2001. "The Representation of Snow in Land Surface Schemes: Results from PILPS 2(d)." *J. Hydrometeorol.* 2 (1): 7–25.

"SNTHERM." 2012. https://www.erdc.usace.army.mil/Media/Fact-Sheets/Fact-Sheet-Article-View/Article/476650/sntherm/.

Steinbrich, Andreas, Markus Weiler, and Hannes Leistert. 2021. "RoGeR – Ein Bodenhydrologisches Modell für Die Beantwortung Einer Vielzahl Hydrologischer Fragen." *In Korrespondenz*

Wasserwirtschaft, 14. Jahrgang 2 (February).

Strasser, U, M Bernhardt, M Weber, G E Liston, and W Mauser. 2008. "Is Snow Sublimation Important in the Alpine Water Balance?" *Cryosphere* 2 (1): 53–66.

Techel, F, and C Pielmeier. 2011. "Point Observations of Liquid Water Content in Wet Snow – Investigating Methodical, Spatial and Temporal Aspects." *Cryosphere* 5 (2): 405–18.

Toreti, A, C Di Ciollo, A Hrast Essenfelder, W Maetens, D Magni, D Masante, M Mazzeschi, et al. 2022. "Drought in Europe August 2022." Publications Office of the European Union; Publications Office of the European Union.

US-Army-Corps-of-Engineers. 1956. "Snow Hydrology: Summary Report of the Snow Investigations, North Pacific Division, Portland, Oregon."

Valery, Audrey. 2010. "Modélisation Précipitations – débit Sous Influence Nivale Elaboration d'un Module Neige Et évaluation Sur 380 Bassins Versants." Edited by Vazken Andreassian. PhD thesis, L'Institut des Sciences et Industries du Vivant et de l'Environnement.

Voordendag, Annelies, Marion Réveillet, Shelley MacDonell, and Stef Lhermitte. 2021. "Snow Model Comparison to Simulate Snow Depth Evolution and Sublimation at Point Scale in the Semi-Arid Andes of Chile." *Cryosphere* 15 (9): 4241–59.

Weiler, Markus. 2023. Edited by Immanuel Frenzel. personal communication.

Whiteman, David, and Rolando Garibotti. 2013. "Rime Mushrooms on Mountains: Description, Formation, and Impacts on Mountaineering." *Bull. Am. Meteorol. Soc.* 94 (9): 1319–27.

Wickham, Hadley, Mara Averick, Jennifer Bryan, Winston Chang, Lucy D'agostino McGowan, Romain François, Garrett Grolemund, et al. 2019. "Welcome to the tidyverse." *Journal of Open Source Software*.

Winkler, Michael, Harald Schellander, and Stefanie Gruber. 2021. "Snow Water Equivalents Exclusively from Snow Depths and Their Temporal Changes: The Δsnow Model." *Hydrol. Earth Syst. Sci.* 25 (3): 1165–87.

Yang, Yang, Theodore A Endreny, and David J Nowak. 2011. "ITree-hydro: Snow Hydrology Update for the Urban Forest Hydrology Model1." *J. Am. Water Resour. Assoc.* 47 (6): 1211–18.

Zheng, Zeshi, Qin Ma, Kun Qian, and Roger C Bales. 2018. "Canopy Effects on Snow Accumulation: Observations from Lidar, Canonical-View Photos, and Continuous Ground Measurements from Sensor Networks." *Remote Sensing* 10 (11): 1769.

Zhibang, Lv, and John W Pomeroy. 2020. "Assimilating Snow Observations to Snow Interception Process Simulations." *Hydrol. Process.* 34 (10): 2229–46.

Zhu, Hao. 2021. “kableExtra: Construct Complex Table with ’Kable’ and Pipe Syntax.”

7 Appendix

7.1 Climate Graphs

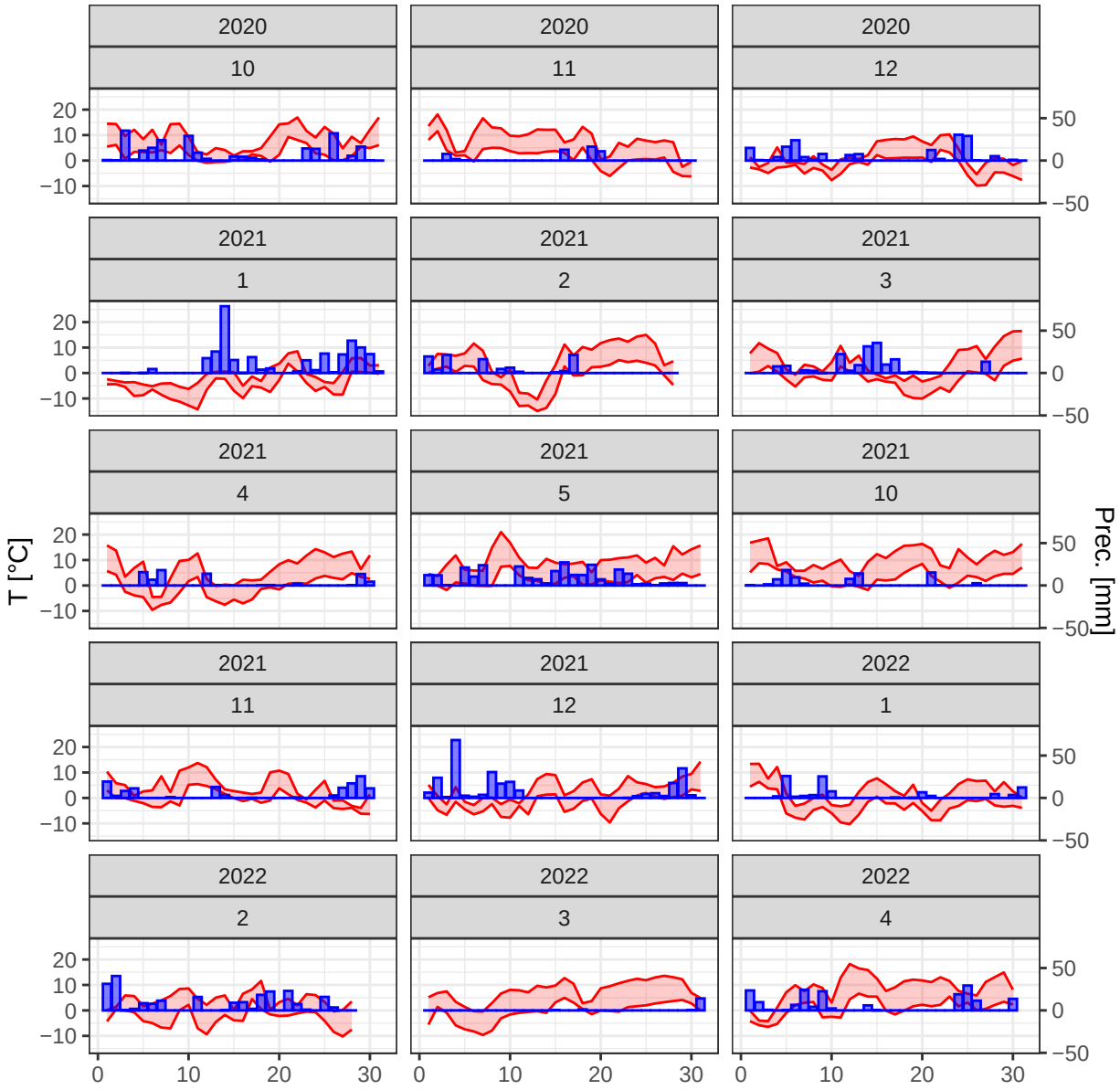

Figure 11: Climate graphs for the winter seasons 2020/21 and 2021/22. Precipitation before Richter correction is plotted (blue). Minimum and maximum daily temperature is shown in red.

7.2 Increase in Precipitation through Richter Correction

Table 12: Precepitation values before and after Richter correction.

Season	Prec. [mm]	Richter Prec. [mm]	Increase [\%]
2020/21	918.6	1077.0	17.2
2021/22	845.8	990.8	17.1

7.3 Development of the DDF

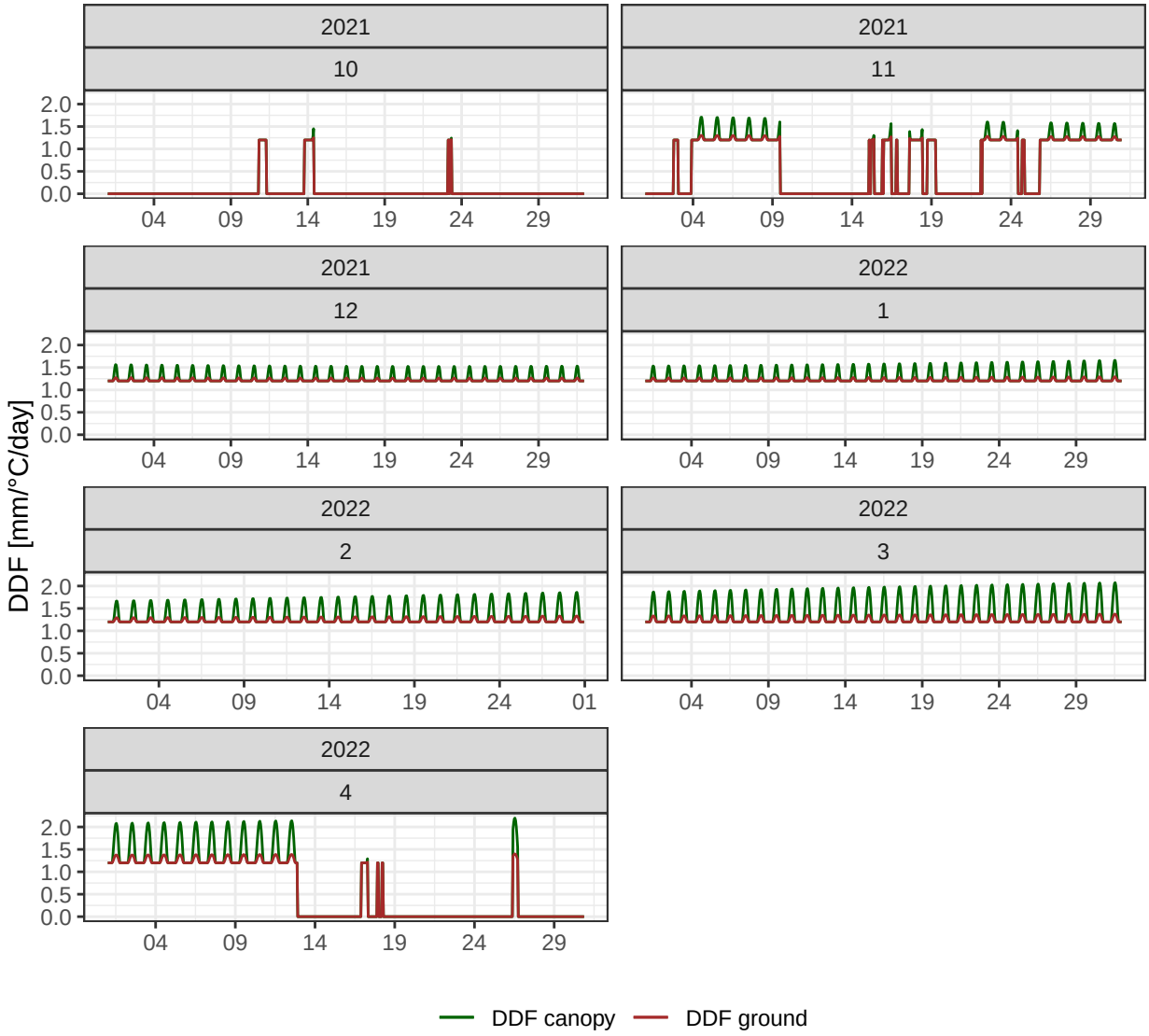

Figure 12: Variation of the DDF in the winter 2021/22 season derived from the open exposed cluster model run. No DDF is calulated when the snow module is turned off. Two different DDF values are calculated for canopy (green) and ground (brown) layer.

7.4 Sensitivity Analysis

Table 13: Appendix: Parameter data intervals for sensitivity analysis.

variable_name	min_value	max_value
storage_coef	0.04	0.12
unloading_factor	0.01	0.20
canopy_coverage	0.00	1.00
ddf	1.00	2.00
t_snowfall	-0.40	2.40
shade	0.00	1.00
lai	2.00	5.00
refreezing_rate	0.05	1.00

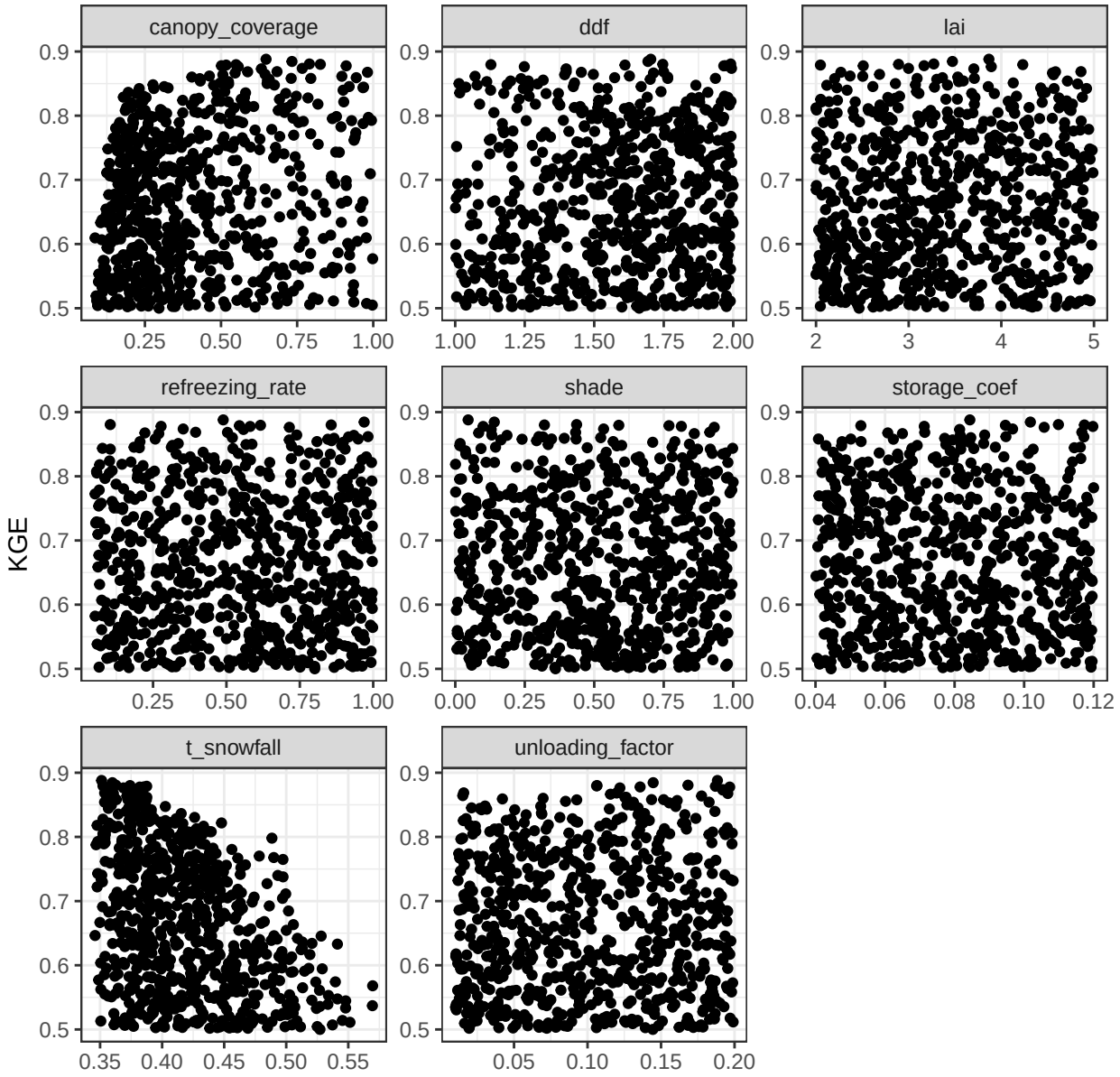

Figure 13: Dotty plots for 50000 model runs with random parameter selection using the Monte Carlo Method. Parameters vary randomly as shown in the table above. For KGE calculation the open-shaded cluster hourly temperature timeseries from 2020/21 is used.

7.5 List of supplied Data and Scripts

- Clima input data (hourly and daily) derived from Raw-climate data with the corresponding script (ClimaInput)
- Images taken from SnoMoS stations and a time-series with manual derived canopy snow cover data (SnoMoS)
- Two file obtained from Geissler, Rathmann, and Weiler (2023) containing manual snow measurements labelled with the corresponding clusters for winter season 2020/2021 and 2021/2022 (ManuelSWEMeasurements)
- A time-series containing the mean SWE together with the standard deviation within each cluster derived from Raw-data modelled by Geissler, Rathmann, and Weiler (2023) with the corresponding script (SpatialSWE)
- A final ready to use version (v26) of the snow module function with additional script for reading inputs, writing outputs and execution (SnowModule)
- Data of 8 simulations with daily and hourly temperature input for the 2020/2021 and 2021/2022 winter seasons for all four clusters (ModelOutput)
- A data-set containing 50000 model runs with varying input parameters for the 2020/2021 and 2021/2022 winter seasons used for sensitivity analysis and a script for dotty plot analysis. The data-set is split in parts of 2000 runs. Hourly temperature input is used. A python script for creating multiple model runs with varying input is provided aswell (SensitivityAnalysis)
- The RMarkdown source file used to create this thesis (Thesis)

7.6 Abbreviations

DDF - Degree Day Factor

ESM- Earth System Models

FSM - Flexible Snow Model

HS - Snow Depth

KGE - Kling Gupta Efficiency

LAI - Leaf Area Index

LiDAR - Light Detection and Ranging

MAE - Mean Absolute Error

m.a.s.l - Meters Above Sea Level

NSE - Nash-Sutcliffe Efficiency

RMSE - Root Mean Squared Error

RoGeR - Runoff Generation Research

ROS - Rain on Snow

SWE - Snow Water Equivalent

SnoMoS - Snow Measuring Station

SNOW-MIP - Snow Model Intercomparison

UAV - Unmanned Aerial Vehicle

8 Statutory Declaration

I hereby declare that this work was done independently and only with the use of the specified resources.

Place, Date Signature

Department of Hydrology

The Albert-Ludwigs-University Of Freiburg i. Brsg.

By

IMMANUEL FRENZEL

Development of a Snow Module for RoGeR utilizing Clustered Snow Data

Under the direction of Dr. Prof. Markus Weiler

Supervised by Joschka Geissler

Freiburg i. Brsg., September 2023